Charged Higgs boson contribution to $B_q^- \to \ell\bar{\nu}$ and $\bar{B} \to (P,V)\ell\bar{\nu}$ in a generic two-Higgs doublet model

Chuan-Hung Chen[1,*] and Takaaki Nomura[2,†]

[1]Department of Physics, National Cheng-Kung University, Tainan 70101, Taiwan
[2]School of Physics, KIAS, Seoul 02455, Korea

(Received 6 March 2018; revised manuscript received 27 September 2018; published 8 November 2018)

We comprehensively study the charged Higgs boson contributions to the leptonic $B_q^- \to \ell\bar{\nu}$ ($q = u, c$) and semileptonic $\bar{B} \to X_q\ell\bar{\nu}$ ($X_u = \pi, \rho$; $X_c = D, D^*$) decays in the type-III two-Higgs doublet model. We employ the Cheng-Sher ansatz to suppress the tree-level flavor-changing neutral currents in the quark sector. When the strict constraints from the $\Delta B = 2$, $b \to s\gamma$, and $pp(b\bar{b}) \to H/A \to \tau^+\tau^-$ processes are considered, parameters χ^u_{tq} from the quark couplings and χ^ℓ_ℓ from the lepton couplings dictate the leptonic and semileptonic B decays. It is found that, when the measured $B_u^- \to \tau\bar{\nu}$ and indirect bound of $B_c^- \to \tau\bar{\nu}$ obtained by LEP1 data are taken into account, $R(D)$ and $R(\pi)$ can have broadly allowed ranges; however, the values of $R(\rho)$ and $R(D^*)$ are limited to approximately the standard model (SM) results. We also find that the same behaviors also occur in the τ-lepton polarizations and forward-backward asymmetries ($A_{FB}^{X_q,\tau}$) of the semileptonic decays, with the exception of $A_{FB}^{D^*,\tau}$, for which the deviation from the SM due to the charged Higgs boson effect is still sizable. In addition, the q^2-dependent $A_{FB}^{\pi,\tau}$ and $A_{FB}^{D,\tau}$ can be very sensitive to the charged Higgs boson effects and have completely different shapes from the SM.

DOI: 10.1103/PhysRevD.98.095007

I. INTRODUCTION

In spite of the success of the standard model (SM) in particle physics, we are still uncertain as to the solutions for baryogenesis, neutrino mass, and dark matter. It is believed that the SM is an effective theory at the electroweak scale, and thus there should be plenty of room to explore the new physics effects in theoretical and experimental high-energy physics.

A known extension of the SM is the two-Higgs doublet model (2HDM), where the model can be used to resolve weak and strong CP problems [1,2]. Because of the involvement of new scalars, such as one CP-even, one CP-odd, and two charged Higgs bosons, despite its original motivation, the 2HDM provides rich phenomena in particle physics [3–6], especially, the charged Higgs boson, which causes lots of interesting effects in flavor physics. According to the imposed symmetry (e.g., soft Z_2 symmetry) to the Lagrangian in the literature, the 2HDM is classified as type-I, type-II, lepton-specific, and flipped models, for which a detailed introduction can be found in Ref. [7]. Among these 2HDM schemes, only the type-II model corresponds to the tree-level minimal supersymmetric standard model (MSSM) case.

Recently, lepton-flavor universality has suffered challenges from tree-level B-meson decays. For instance, *BABAR* [8,9], Belle [10–12], and LHCb [13,14] observed unexpected large branching ratios (BRs) in $\bar{B} \to D^{(*)}\tau\bar{\nu}_\tau$, and the averaged observables were defined and measured as [15]

$$R(D) = \frac{\mathrm{BR}(\bar{B} \to D\tau\bar{\nu})}{\mathrm{BR}(\bar{B} \to D\ell\bar{\nu})} = 0.407 \pm 0.039 \pm 0.024,$$
$$R(D^*) = \frac{\mathrm{BR}(\bar{B} \to D^*\tau\bar{\nu})}{\mathrm{BR}(\bar{B} \to D^*\ell\bar{\nu})} = 0.304 \pm 0.013 \pm 0.007, \quad (1)$$

where ℓ denotes the light leptons, and the SM predictions using different approaches are closed to each other and obtained as $R(D) \approx 0.30$ [16–19] and $R(D^*) \approx 0.25$ [18–21]. Intriguingly, when the $R(D) - R(D^*)$ correlation is taken into account, the deviation with respect to the SM prediction is 4.1σ. Based on these observations, possible extensions of the SM for explaining the excesses are studied in Refs. [22–66].

Moreover, when $|V_{ub}| \approx 3.72 \times 10^{-3}$ is taken from the results of lattice QCD [67] and light-cone sum rules (LCSRs) [68,69], the SM result of $\mathrm{BR}(B_u^- \to \tau\bar{\nu})^{\mathrm{SM}} \approx 0.89 \times 10^{-4}$ is

*physchen@mail.ncku.edu.tw
†nomura@kias.re.kr

slightly smaller than the current measurement of $\mathrm{BR}(B_u^- \to \tau\bar{\nu})^{\mathrm{exp}} = (1.09 \pm 0.24) \times 10^{-4}$ [70]. In addition to the uncertainties of V_{ub} and B-meson decay constant f_B, the difference between the SM prediction and experimental data may raise from new charged current effects [71–74]. Since the $\bar{B} \to D^{(*)}\tau\bar{\nu}$ and $B_u^- \to \tau\bar{\nu}$ processes are associated with the $W^{\pm}$-mediated $b \to (u, c)\tau\bar{\nu}$ decays in the SM, in this work, we study the charged Higgs boson contributions to the decays in detail in the 2HDM framework.

The charged Higgs boson can be naturally taken as the origin of a lepton-flavor universality violation, because its Yukawa coupling to a lepton is usually proportional to the lepton mass. Because of the suppression of m_ℓ/v ($v \approx 246$ GeV), we thus need an extra factor in the coupling to enhance the charged Higgs boson effect. In the 2HDM schemes mentioned above, it can be easily found that only the type-II model can have a $\tan^2\beta$ enhancement in the Hamiltonian of $b \to (u, c)\tau\bar{\nu}$. However, the type-II 2HDM cannot resolve the excesses for the following reasons: (i) The sign of type-II contribution is always destructive to the SM contributions in $b \to (u, c)\tau\bar{\nu}$, and (ii) the lower bound of the charged Higgs mass limited by $b \to s\gamma$ is now $m_{H^\pm} > 580$ GeV [75], so that the change due to the charged Higgs boson effect is only at a percentage level. Inevitably, we have to consider other schemes in the 2HDM that can retain the $\tan\beta$ enhancement, can be a constructive contribution to the SM, and can have a smaller $m_{H^\pm}$.

The desired scheme can be achieved when the imposed symmetry is removed; that is, the two Higgs doublets can simultaneously couple to the up- and down-type quarks. This scheme is called the type-III 2HDM in the literature [5,23,28]. In such a scheme, unless an extra assumption is made [76], the flavor-changing neutral currents (FCNCs) are generally induced at the tree level. In order to naturally suppress the tree-induced $\Delta F = 2$ ($F = K$, $B_{d(s)}$, D) processes, we can adopt the Cheng-Sher ansatz [77], where the FCNC effects are parametrized to be the square root of the production involving flavor masses. We find that the same quark FCNC effects also appear in the charged Higgs couplings to the quarks. Using the Cheng-Sher ansatz, it is found that, in addition to the achievements of the $\tan\beta$ enhancement factor and a smaller $m_{H^\pm}$, new unsuppressed factors denoted by $\chi^u_{tc(tu)}$ occur at the vertices $c(u)bH^\pm$, which play an important role in $B_u^- \to \tau\bar{\nu}$ and $R(D^{(*)})$. We note that the type-II 2HDM and MSSM can generate the similar Yukawa couplings of the type-III model through the Z_2 soft-breaking term, which is from the Higgs potential, when loop effects are considered. Because of the loop suppression factor, the loop-induced effects from type-II 2HDM in our study are small. Although the loop effects in supersymmetric (SUSY) models could be sizable, since we focus on the non-SUSY models, the implications of loop-induced FCNCs in MSSM can be found in Refs. [78–81].

With the full $\Upsilon(4S)$ data set, Belle recently reported the measurement of $B_u^- \to \mu\bar{\nu}$ with a 2.4σ significance, where the corresponding BR is $\mathrm{BR}(B_u^- \to \mu\bar{\nu})^{\mathrm{exp}} = (6.46 \pm 2.22 \pm 1.60) \times 10^{-7}$, and the SM result is $\mathrm{BR}(B_u^- \to \mu\bar{\nu})^{\mathrm{SM}} = (3.8 \pm 0.31) \times 10^{-7}$ [82]. The experimental measurement approaches the SM prediction, and it is expected that the improved measurement soon will be obtained at Belle II [83]. In other words, in addition to the $B_u^- \to \tau\bar{\nu}$ channel, we can investigate the new charged current effect through a precise measurement on the $B_u^- \to \mu\bar{\nu}$ decay.

In order to comprehensively understand the charged Higgs boson contributions to the $b \to (u, c)\ell\bar{\nu}$ ($\ell = e, \mu, \tau$) in the type-III 2HDM, in addition to the chiral suppression channels $B_u^- \to (\tau, \mu)\bar{\nu}$, we study various possible observables for the semileptonic processes $\bar{B} \to (P, V)\ell\bar{\nu}$ ($P = \pi$, D; $V = \rho$ D^*), which include BRs, $R(P)$, $R(V)$, lepton helicity asymmetry, and lepton forward-backward asymmetry. To constrain the free parameters, we study not only the constraints from the tree- and loop-induced $\Delta B = 2$ processes but also the $b \to s\gamma$ decay, which has arisen from the new neutral scalars and charged Higgs boson. Although the neutral current contributions to $b \to s\gamma$ are much smaller than those from the charged Higgs boson, for completeness, we also formulate their contributions in the paper. In addition, the upper bound of $\mathrm{BR}(B_c^- \to \tau\bar{\nu}) < 10\%$ obtained in Ref. [65] is also taken into account when we investigate the $\bar{B} \to D^*\tau\bar{\nu}$ decay.

LHCb reported more than a 2σ deviation from the SM in $R(K) = \mathrm{BR}(B^+ \to K^+\mu^+\mu^-)/\mathrm{BR}(B^+ \to K^+e^+e^-) = 0.745^{+0.090}_{-0.074} \pm 0.036$ [84] and $R(K^*) = \mathrm{BR}(B^0 \to K^{*0}\mu^+\mu^-)/\mathrm{BR}(B^0 \to K^{*0}e^+e^-) = 0.69^{+0.11}_{-0.07} \pm 0.05$ [85]. Since we concentrate on the tree-level leptonic and semileptonic B decays, we do not address this issue in this work. The charged Higgs boson contributions to the $b \to s\ell^+\ell^-$ processes can be found in Refs. [86–91].

The paper is organized as follows: In Sec. II, we discuss and parametrize the charged Higgs Yukawa couplings to the quarks and leptons in the type-III 2HDM. In Sec. III, we study the charged Higgs boson contributions to the leptonic $B^-_{u(c)} \to \ell\bar{\nu}$ and $\bar{B} \to (P, V)\ell\bar{\nu}$ decays, where the interesting potential observables include the decay rate, the branching fraction ratio, lepton helicity asymmetry, and lepton forward-backward asymmetry. We study the tree- and loop-induced $\Delta B = 2$ and loop-induced $b \to s\gamma$ processes in Sec. IV, where the contributions of neutral scalar H, neutral pseudoscalar A, and the charged Higgs boson are taken into account. The detailed numerical analysis and the current experimental bounds are shown in Sec. V, and a conclusion is given in Sec. VI.

II. YUKAWA COUPLINGS IN THE GENERIC 2HDM

To study the charged Higgs boson contributions to the $b \to q\ell\bar{\nu}$ ($q = u$, c) decays in the type-III 2HDM, we

analyze the relevant Yukawa couplings in this section, especially, the charged Higgs couplings to ub and cb, where they can make significant contributions to the leptonic and semileptonic B decays. The characteristics of new Yukawa couplings in the type-III model will be also discussed.

A. Formulation of $H^\pm$ Yukawa couplings to the quarks and leptons

Since the charged Higgs couplings to the quarks and the leptons in type-III 2HDM were derived before [5], we briefly introduce the relevant pieces in this section. We begin to write the Yukawa couplings in the type-III model as

$$\begin{aligned}-\mathcal{L}_Y &= \bar{Q}_L Y_1^d D_R H_1 + \bar{Q}_L Y_2^d D_R H_2 + \bar{Q}_L Y_1^u U_R \tilde{H}_1 \\ &\quad + \bar{Q}_L Y_2^u U_R \tilde{H}_2 + \bar{L} Y_1^\ell \ell_R H_1 \\ &\quad + \bar{L} Y_2^\ell \ell_R H_2 + \text{H.c.}, \end{aligned} \tag{2}$$

where the flavor indices are suppressed; $Q_L^T = (u, d)_L$ and $L^T = (\nu, \ell)_L$ are the $SU(2)_L$ quark and lepton doublets, respectively; f_R ($f = U, D, \ell$) is the singlet fermion; $Y_{1,2}^f$ are the 3×3 Yukawa matrices, and $\tilde{H}_i = i\tau_2 H_i^*$ with τ_2 being the Pauli matrix. The components of the Higgs doublets are taken as

$$H_i = \begin{pmatrix} \phi_i^+ \\ (v_i + \phi_i + i\eta_i)/\sqrt{2} \end{pmatrix}, \tag{3}$$

and v_i is the vacuum expectation value of H_i. We note that Eq. (2) can recover the type-II 2HDM when Y_1^u, Y_2^d, and Y_2^ℓ vanish. The physical states for scalars can then be expressed as

$$\begin{aligned} h &= -s_\alpha \phi_1 + c_\alpha \phi_2, \qquad H = c_\alpha \phi_1 + s_\alpha \phi_2, \\ H^\pm(A) &= -s_\beta \phi_1^\pm(\eta_1) + c_\beta \phi_2^\pm(\eta_2), \end{aligned} \tag{4}$$

where the mixing angles are defined as $c_\alpha(s_\alpha) = \cos\alpha(\sin\alpha)$, $c_\beta = \cos\beta = v_1/v$, and $s_\beta = \sin\beta = v_2/v$ with $v = \sqrt{v_1^2 + v_2^2}$. In this work, h is the SM-like Higgs boson while H, A, and $H^\pm$ are new scalar bosons.

The fermion mass matrix can be formulated as

$$\bar{f}_L \mathbf{M}^f f_R + \text{H.c.} \equiv \frac{v}{\sqrt{2}} \bar{f}_L (c_\beta Y_1^f + s_\beta Y_2^f) f_R + \text{H.c.} \tag{5}$$

Without assuming the relation between Y_1^f and Y_2^f, both Yukawa matrices cannot be simultaneously diagonalized [76]. Thus, the FCNCs mediated by scalar bosons are induced at the tree level. We introduce unitary matrices U_L^f and U_R^f to diagonalize the fermion mass matrices by following $f_L^p = U_L^f f_L^w$ and $f_R^p = U_R^f f_R^w$, where $f_{L,R}^{p(w)}$ denote the physical (weak) eigenstates. Then, the Yukawa couplings of $H^\pm$ can be written as [5]

$$\begin{aligned} -\mathcal{L}_Y^{H^\pm} &= \sqrt{2}\bar{u}_R \left[-\frac{1}{v t_\beta} \mathbf{m_u} + \frac{\mathbf{X}^{u\dagger}}{s_\beta} \right] \mathbf{V} d_L H^+ \\ &\quad + \sqrt{2}\bar{u}_L \mathbf{V} \left[-\frac{t_\beta}{v} \mathbf{m_d} + \frac{\mathbf{X}^d}{c_\beta} \right] d_R H^+ \\ &\quad + \sqrt{2}\bar{\nu}_L \left[-\frac{\tan\beta}{v} \mathbf{m}_\ell + \frac{\mathbf{X}^\ell}{c_\beta} \right] \ell_R H^+ + \text{H.c.}, \end{aligned} \tag{6}$$

where $t_\beta = \tan\beta = v_2/v_1$; $\mathbf{V} \equiv U_L^u U_L^{d\dagger}$ denotes the Cabibbo-Kobayashi-Maskawa (CKM) matrix, and the $\mathbf{X}$'s are defined as

$$\mathbf{X}^u = U_L^u \frac{Y_1^u}{\sqrt{2}} U_R^{u\dagger}, \quad \mathbf{X}^d = U_L^d \frac{Y_2^d}{\sqrt{2}} U_R^{d\dagger}, \quad \mathbf{X}^\ell = U_L^\ell \frac{Y_2^\ell}{\sqrt{2}} U_R^{\ell\dagger}. \tag{7}$$

$\mathbf{X}^{u,d}$ are the sources of tree-level FCNCs in the type-III model. In order to accommodate the strict constraints from the $\Delta F = 2$ processes, such as Δm_P ($P = K, B_{d,s}, D$), we adopt the so-called Cheng-Sher ansatz [77] in the quark and lepton sectors, where $\mathbf{X}^f$ is parametrized as

$$X_{ij}^f = \frac{\sqrt{m_{f_i} m_{f_j}}}{v} \chi_{ij}^f \tag{8}$$

and χ_{ij}^f are the new free parameters. Using this ansatz, it can be seen that Δm_P arisen from the tree level is suppressed by $m_d m_s/v^2$ for the K meson, $m_{d(s)} m_b/v^2$ for $B_{d(s)}$, and $m_u m_c/v^2$ for the D meson. Since we do not study the origin of neutrino mass, the neutrinos are taken as massless particles in this work. Nevertheless, even with a massive neutrino case, the influence on hadronic processes is small and negligible. In addition, to simplify the numerical analysis, in this work we use the scheme with $\mathbf{X}_{ij}^\ell = (m_{\ell_i}/v)\chi_{\ell_i}^\ell \delta_{\ell_i \ell_j}$, i.e., $\chi_{\ell_i \ell_j}^\ell = \chi_{\ell_i}^\ell \delta_{\ell_i \ell_j}$; as a result, the Yukawa couplings of $H^\pm$ to the leptons can be expressed as

$$\mathcal{L}_{Y,\ell}^{H^\pm} = \sqrt{2}\frac{\tan\beta m_\ell}{v} \left(1 - \frac{\chi_\ell^\ell}{s_\beta} \right) \bar{\nu}_\ell P_R \ell H^+ + \text{H.c.}, \tag{9}$$

with $P_{R(L)} = (1 \pm \gamma_5)/2$. The suppression factor m_ℓ/v could be moderated using the scheme of large $\tan\beta$.

B. b-quark Yukawa couplings to $H^\pm$

From Eq. (6), it can be seen that the coupling $u_{iR} b_L H^\pm$ ($u_i = u, c$) in the type-II 2HDM (i.e., $\mathbf{X}^{d,u} = 0$) is suppressed by $m_{u_i}/(v t_\beta) V_{u_i b}$, and this effect can be neglected. However, the situation is changed in the type-III model.

In addition to the disappearance of suppression factor $1/t_\beta$, the new effect $\mathbf{X}^u$ accompanied with the CKM matrix in the form of $\mathbf{X}^u V/v$ could lead to $\sqrt{m_{u_i} m_t}/v \chi^u_{u_i t} V_{tb}$, where $\sqrt{m_{u_i} m_t}/v$ numerically plays the role of $|V_{u_i b}|$ and the magnitude of the coupling is dictated by the free parameter $\chi^u_{u_i t}$, which, in principle, is not suppressed. Additionally, the $u_{iL} b_R H^\pm$ coupling is also remarkably modified. In order to better comprehend the influence of the new charged Higgs couplings on the B decays, in the rest of this subsection, we discuss the $u_i b H^\pm$ coupling in detail. For convenience, we rewrite the $H^\pm$ couplings to the b quark and light up-type quarks as

$$\begin{aligned}
&\mathcal{L}_Y^{H^\pm} \supset \frac{\sqrt{2}}{v} \bar{u}_{iR} C^L_{u_i b} b_L H^+ + \frac{\sqrt{2}}{v} \bar{u}_{iL} C^R_{u_i b} b_R H^+ + \text{H.c.},\\
&C^L_{u_i b} = \left(\frac{m_{u_i}}{t_\beta} \delta_{u_i u_j} - \frac{\sqrt{m_{u_i} m_{u_j}}}{s_\beta} \chi^{u*}_{u_j u_i} \right) V_{u_j b},\\
&C^R_{u_i b} = V_{u_i d_j} \left(t_\beta m_b \delta_{d_j b} - \frac{\sqrt{m_{d_j} m_b}}{c_\beta} \chi^d_{d_j b} \right),
\end{aligned} \tag{10}$$

where u_j (d_j) indicates the sum of all possible up- (down-) type quarks.

In the following, we analyze the characteristics of the $C^L_{u(c)b}$ and $C^R_{u(c)b}$ couplings in the type-III 2HDM with the Cheng-Sher ansatz. Because of $m_u V_{ub} \ll \sqrt{m_u m_c} V_{cb} \ll \sqrt{m_u m_t} V_{tb}$, we can simplify the C^L_{ub} coupling as

$$\frac{\sqrt{2}}{v} C^L_{ub} \approx -\sqrt{2} \frac{\sqrt{m_u m_t}}{v s_\beta} \chi^{u*}_{tu} V_{tb}. \tag{11}$$

With $m_u \sim 5.4$ MeV, $m_t \sim 165$ GeV, and $v \approx 246$ GeV, it can be found that $\sqrt{m_u m_t}/v \approx 3.84 \times 10^{-3}$ is very close to the value of $|V_{ub}|$; therefore, C^L_{ub} can be read as $\sqrt{2} C^L_{ub}/v \sim -\sqrt{2} \chi^{u*}_{tu} |V_{ub}|$, where $s_\beta \approx 1$ is applied. Clearly, unlike the case in the type-II 2HDM, which is highly suppressed by $m_u/(v t_\beta)$, C^L_{ub} in the type-III model is still proportional to $|V_{ub}|$, can be sizable, and is controlled by χ^{u*}_{tu}. For the C^R_{ub} coupling, the decomposition from Eq. (10) can be written as

$$\begin{aligned}
C^R_{ub} = &-V_{ud} \frac{\sqrt{m_d m_b} \chi^d_{db}}{c_\beta} - V_{us} \frac{\sqrt{m_s m_b} \chi^d_{sb}}{c_\beta}\\
&+ V_{ub} m_b \left(t_\beta - \frac{\chi^d_{bb}}{c_\beta} \right).
\end{aligned} \tag{12}$$

The numerical values of the first two terms can be obtained as $V_{ud}\sqrt{m_d/m_b} \approx 0.047$ and $V_{us}\sqrt{m_s/m_b} \approx 0.032 \gg |V_{ub}|$. Unless $\chi^d_{db,sb}$ are strictly constrained, each term with different CKM factors may be important and cannot be arbitrarily dropped. For clarity, we rewrite C^R_{ub} to be

$$\frac{\sqrt{2}}{v} C^R_{ub} = \sqrt{2} \frac{m_b t_\beta}{v} V_{ub} \left(1 - \frac{\chi^R_{ub}}{s_\beta} \right), \tag{13}$$

$$\chi^R_{ub} = \chi^d_{bb} + \frac{V_{ud}}{V_{ub}} \sqrt{\frac{m_d}{m_b}} \chi^d_{db} + \frac{V_{us}}{V_{ub}} \sqrt{\frac{m_s}{m_b}} \chi^d_{sb}. \tag{14}$$

Because of $|V_{ub}| \ll V_{us,ud}$, the magnitude of χ^R_{ub}, in principle, can be of $O(10)$, and the resulting C^R_{ub} is much larger than that in the type-II 2HDM. In order to avoid obtaining an C^R_{ub} that is too large, we can require a cancellation between $V_{ud}\sqrt{m_d/m_b}\chi^d_{db}$ and $V_{us}\sqrt{m_s/m_b}\chi^d_{sb}$ when $\chi^d_{db,sb}$ both are sizable. However, we will show that $\chi^d_{db,sb}$ indeed are constrained by the measured $B_{d,s}$ mixing parameters and that their magnitudes should be less than $O(10^{-2})$.

For the processes dictated by the $b \to c$ decays, due to $\sqrt{m_u m_c} V_{ub} \ll m_c V_{cb} \ll \sqrt{m_c m_t} V_{tb}$, the $H^\pm$ Yukawa coupling of C^L_{cb} can be simplified as

$$\begin{aligned}
\frac{\sqrt{2}}{v} C^L_{cb} &\approx -\frac{\sqrt{2}}{v} \frac{\sqrt{m_c m_t}}{s_\beta} \chi^{u*}_{tc} V_{tb}\\
&= -\sqrt{2} \frac{m_t}{v} V_{cb} \left(\frac{\chi^{u*}_{tc}}{s_\beta} \sqrt{\frac{m_c}{m_t}} \frac{V_{tb}}{V_{cb}} \right),
\end{aligned} \tag{15}$$

where the m_c/t_β term has been ignored due to the use of large t_β scheme and the factor in parentheses can be numerically estimated to be $2.19\chi^{u*}_{tc}$. This behavior is similar to C^L_{ub}, but it is χ^{u*}_{tc} that controls the magnitude. Clearly, if χ^{u*}_{tc} is not suppressed, it can make a significant contribution to the $b \to c$ transition. Using the fact that $|V_{cd}|\sqrt{m_d m_b} \ll V_{sc}\sqrt{m_s m_b}$, $V_{cb} m_b$, we can formulate the C^R_{cb} coupling as

$$\begin{aligned}
&\frac{\sqrt{2}}{v} C^R_{cb} \approx \sqrt{2} \frac{m_b t_\beta}{v} V_{cb} \left(1 - \frac{\chi^R_{cb}}{s_\beta} \right),\\
&\chi^R_{cb} = \chi^d_{bb} + \sqrt{\frac{m_s}{m_b}} \frac{V_{cs}}{V_{cb}} \chi^d_{sb} \approx \chi^d_{bb} + 3.69 \chi^d_{sb}.
\end{aligned} \tag{16}$$

Since C^R_{cb} has the t_β enhancement, its magnitude is comparable with the SM W-gauge coupling of $g V_{cb}/\sqrt{2}$. For comparison, we also show the $tbH^\pm$ couplings as

$$\frac{\sqrt{2}}{v} C^L_{tb} \approx \sqrt{2} \frac{m_t}{v} V_{tb} \left(\frac{1}{t_\beta} - \frac{\chi^{u*}_{tt}}{s_\beta} \right), \tag{17}$$

$$\frac{\sqrt{2}}{v} C^R_{tb} \approx \sqrt{2} \frac{m_b t_\beta}{v} V_{tb} \left(1 - \frac{\chi^d_{bb}}{s_\beta} \right), \tag{18}$$

where the small effects related to $V_{ub,cb}$ and $V_{ts,td}$ have been dropped. Although there is an m_t enhancement in the first term of C_{tb}^{L}, $1/t_\beta$ will reduce its contribution when a large $\tan\beta$ value is taken; therefore, comparing with χ_{tt}^{u*}/s_β, this term can be ignored, i.e., $C_{tb}^{L} \approx -m_t V_{tb}\chi_{tt}^{u*}/s_\beta$. From the above analysis, it can be seen that $C_{ub,cb,tb}^{L,R}$ are different from those in the type-II model not only in magnitude but also in sign. For completeness, the other Yukawa couplings of $H^\pm$ to the quarks are shown in detail in the Appendix.

III. PHENOMENOLOGICAL ANALYSIS

The charged current interactions in this model arise from the SM W-gauge and the charged Higgs bosons. Based on the Yukawa couplings in Eqs. (9) and (10), the effective Hamiltonian for $b \to q\ell\bar{\nu}$ can be written as

$$\begin{aligned}\mathcal{H}(b \to q\ell\bar{\nu}) = \frac{G_F}{\sqrt{2}} V_{qb}\Big[&(\bar{q}b)_{V-A}(\bar{\ell}\nu)_{V-A} \\ &+ C_{qb}^{L,\ell}(\bar{q}b)_{S-P}(\bar{\ell}\nu)_{S-P} \\ &+ C_{qb}^{R,\ell}(\bar{q}b)_{S+P}(\bar{\ell}\nu)_{S-P}\Big],\end{aligned} \tag{19}$$

where the fermionic currents are defined as $(\bar{f}'f)_{V\pm A} = \bar{f}'\gamma^\mu(1\pm\gamma_5)f$ and $(\bar{f}'f)_{S\pm P} = \bar{f}'(1\pm\gamma_5)f$ and the dimensionless coefficients for the $b \to u$ and $b \to c$ decays are given as

$$C_{ub}^{L,\ell} = \frac{m_t m_\ell t_\beta}{m_{H^\pm}^2 s_\beta}\left(1 - \frac{\chi_\ell^\ell}{s_\beta}\right)\left(\sqrt{\frac{m_u}{m_t}}\frac{V_{tb}}{V_{ub}}\chi_{tu}^{u*}\right), \tag{20a}$$

$$C_{ub}^{R,\ell} = -\frac{m_b m_\ell t_\beta^2}{m_{H^\pm}^2}\left(1 - \frac{\chi_\ell^\ell}{s_\beta}\right)\left(1 - \frac{\chi_{ub}^R}{s_\beta}\right), \tag{20b}$$

$$C_{cb}^{L,\ell} = \frac{m_t m_\ell t_\beta}{m_{H^\pm}^2 s_\beta}\left(1 - \frac{\chi_\ell^\ell}{s_\beta}\right)\left(\sqrt{\frac{m_c}{m_t}}\frac{V_{tb}}{V_{cb}}\chi_{tc}^{u*}\right), \tag{20c}$$

$$C_{cb}^{R,\ell} = -\frac{m_b m_\ell t_\beta^2}{m_{H^\pm}^2}\left(1 - \frac{\chi_\ell^\ell}{s_\beta}\right)\left(1 - \frac{\chi_{cb}^R}{s_\beta}\right). \tag{20d}$$

Based on the interactions shown in Eqs. (19) and (20), we investigate the charged Higgs boson influence on the leptonic and semileptonic B decays in the type-III 2HDM.

A. Leptonic $B_q^- \to \ell\bar{\nu}$ decays

The hadronic effect in a leptonic B decay is the B-meson decay constant. The decay constant associated with an axial-vector current for the B_q-meson is defined as

$$\langle 0|\bar{q}\gamma^\mu\gamma_5 b|B_q^-(p_{B_q})\rangle = -if_{B_q}p_{B_q}^\mu. \tag{21}$$

Using the equation of motion, the decay constant associated with pseudoscalar current is given by

$$\langle 0|\bar{q}\gamma_5 b|B_q^-(p)\rangle = if_{B_q}\frac{m_{B_q}^2}{m_b + m_q}. \tag{22}$$

From the effective interactions in Eq. (19), the decay rate for $B_q^- \to \ell\bar{\nu}$ can be formed as

$$\Gamma(B_q^- \to \ell\bar{\nu}) = \Gamma^{\rm SM}(B_q^- \to \ell\bar{\nu})\left|1 + \frac{m_{B_q}^2(C_{qb}^{R,\ell} - C_{qb}^{L,\ell})}{m_\ell(m_b + m_q)}\right|^2, \tag{23}$$

$$\Gamma^{\rm SM}(B_q^- \to \ell\bar{\nu}) = \frac{G_F^2}{8\pi}|V_{qb}|^2 f_{B_q}^2 m_{B_q} m_\ell^2\left(1 - \frac{m_\ell^2}{m_{B_q}^2}\right)^2. \tag{24}$$

Since a leptonic meson decay is a chirality-suppressed process, the decay rate in Eq. (24) is proportional to m_ℓ^2. From Eqs. (20a)–(20d), it can be seen that, in the type-II 2HDM, $C_{ub}^{L} \sim C_{cb}^{L} \sim 0$ and $C_{ub,cb}^{R}$ are negative in sign; therefore, the $H^\pm$ contribution to the $B_q^- \to \ell\bar{\nu}$ decay is always destructive. The magnitude and the sign of $C_{qb}^{R,L}$ in the type-III model can be changed due to the new effects of $\chi_{ij}^{u,d}$ and $\chi_{\ell'}^{\ell}$,.

Before doing a detailed numerical analysis, we can numerically understand the impact of the 2HDM on the $B_q^- \to \ell\bar{\nu}$ decay as follows: Taking $t_\beta = 50$ and $m_{H^\pm} = 300$ GeV, we can see that the charged Higgs boson contributions to the $b \to u$ and $b \to c$ decays are, respectively, given as

$$\begin{aligned}\delta_q^{H^\pm,\ell} &\equiv \frac{m_{B_q}^2(C_{qb}^{R,\ell} - C_{qb}^{L,\ell})}{m_\ell(m_b + m_q)} \\ &\approx \begin{cases} -[0.77(1 - \chi_{ub}^R/s_\beta) + 0.39\chi_{tu}^{u*}e^{i\phi_3}](1 - \chi_\ell^\ell/s_\beta), \\ -[1.09(1 - \chi_{cb}^R/s_\beta + 1.77\chi_{tc}^{u*})](1 - \chi_\ell^\ell/s_\beta), \end{cases}\end{aligned} \tag{25}$$

where the sign can be positive when the parameters of $\chi_{tu,tc}^{u*}$ and χ_ℓ^ℓ are properly taken and ϕ_3 is the phase in V_{ub}. We note that the Yukawa coupling of the charged Higgs boson to the lepton is proportional to the lepton mass; therefore, the ratio in Eq. (25) does not depend on m_ℓ. The lepton-flavor-dependent effect is dictated by the χ_ℓ^ℓ parameter.

B. $B_q^- \to (P,V)\ell\bar{\nu}$ decays

Since the semileptonic B decays involve the hadronic QCD effects, in order to formulate the decays, we parametrize the form factors for a B decay to a pseudoscalar (P) meson as

$$\langle P(p_2)|\bar{q}\gamma^\mu b|\bar{B}(p_1)\rangle = f_1^{BP}(q^2)\left[P^\mu - \frac{P\cdot q}{q^2}q^\mu\right] + f_0^{BP}(q^2)\frac{P\cdot q}{q^2}q^\mu,$$
$$\langle P(p_2)|\bar{q}b|\bar{B}(p_1)\rangle = (m_B + m_P)f_S^{BP}(q^2), \tag{26}$$

where $P = p_1 + p_2$ and $q = p_1 - p_2$. The form factors for a B decay to a vector (V) meson is defined as

$$\langle V(p_2,\epsilon_V)|\bar{q}\gamma^\mu b|\bar{B}(p_1)\rangle = \frac{V^{BV}(q^2)}{m_B + m_V}\varepsilon^{\mu\nu\rho\sigma}\epsilon^*_{V\nu}P_\rho q_\sigma,$$
$$\langle V(p_2,\epsilon_V)|\bar{q}\gamma^\mu\gamma_5 b|\bar{B}(p_1)\rangle = 2im_V A_0^{BV}(q^2)\frac{\epsilon_V^*\cdot q}{q^2}q^\mu + i(m_B+m_V)A_1^{BV}(q^2)\left[\epsilon_V^{*\mu} - \frac{\epsilon_V^*\cdot q}{q^2}q^\mu\right]$$
$$- iA_2^{BV}(q^2)\frac{\epsilon_V^*\cdot q}{m_B+m_V}\left[P^\mu - \frac{P\cdot q}{q^2}q^\mu\right],$$
$$\langle V(p_2,\epsilon_V)|\bar{q}\gamma_5 b|\bar{B}(p_1)\rangle = -i\epsilon_V^*\cdot q f_P^{BV}(q^2). \tag{27}$$

With the equation of motion, the form factors of f_S^{BP} and f_P^{BV} can be obtained, respectively, as

$$f_S^{BP}(q^2) \approx \frac{m_B - m_P}{m_b - m_q}f_0(q^2), \qquad f_P^{BV}(q^2) \approx \frac{2m_V}{m_b+m_q}A_0(q^2). \tag{28}$$

Using the interactions in Eq. (19) and the form factors defined above, we can obtain the transition matrix elements for $\bar{B}\to(P,V)\ell\bar{\nu}$ as

$$\mathcal{M}_P = \frac{G_F}{\sqrt{2}}V_{qb}\left[f_1^{BP}\left(P^\mu - \frac{P\cdot q}{q^2}q^\mu\right)(\bar{\ell}\nu)_{V-A} + \left(m_\ell f_0^{BP}\frac{P\cdot q}{q^2} + (C_{qb}^{R,\ell} + C_{qb}^{L,\ell})(m_B+m_P)f_S^{BP}\right)(\bar{\ell}\nu)_{S-P}\right], \tag{29}$$

$$\mathcal{M}_V^L = -i\frac{G_F}{\sqrt{2}}V_{qb}\left\{\epsilon_V^*\cdot q\left((C_{qb}^{R,\ell} - C_{qb}^{L,\ell})f_P^{BP} + 2A_0^{BV}\frac{m_V m_\ell}{q^2}\right)(\bar{\ell}\nu)_{S-P}\right.$$
$$\left. + \left[(m_B+m_V)A_1^{BV}\left(\epsilon_{V\mu}^*(L) - \frac{\epsilon_V^*\cdot q}{q^2}q_\mu\right) - \frac{A_2^{BV}\epsilon_V^*\cdot q}{m_B+m_V}\left(P_\mu - \frac{P\cdot q}{q^2}q_\mu\right)\right](\bar{\ell}\nu)_{V-A}\right\},$$
$$\mathcal{M}_V^T = \frac{G_F}{\sqrt{2}}V_{qb}\left[\frac{V^{BV}}{m_B+m_V}\varepsilon_{\mu\nu\rho\sigma}\epsilon_V^{*\nu}(T)P^\rho q^\sigma - i(m_B+m_V)A_1^{BV}\epsilon_{V\mu}^*(T)\right](\bar{\ell}\nu)_{V-A}, \tag{30}$$

where q^2 dependence in the form factors is hidden and $\mathcal{M}_V^L$ and $\mathcal{M}_V^T$ are the longitudinal and transverse V-meson components, respectively. From the formulations, we see that the charged Higgs boson affects only $\mathcal{M}_P$ and the longitudinal part of the V meson.

1. Decay amplitudes in helicity basis

To derive the angular differential decay rate, we take the coordinates of the kinematic variables in the rest frame of the $\ell\bar{\nu}$ invariant mass as

$$q = \left(\sqrt{q^2},0,0,0\right), \qquad p_M = (E_M,0,0,p_M), \qquad p_M = \frac{\sqrt{\lambda_M}}{2\sqrt{q^2}},$$
$$\lambda_M = m_B^4 + m_M^4 + q^4 - 2m_B^2m_M^2 - 2m_B^2q^2 - 2m_M^2q^2,$$
$$p_\nu = E_\nu(1,\sin\theta_\ell\cos\phi,\sin\theta_\ell\sin\phi,\cos\theta_\ell), \qquad p_\ell = (E_\ell,-\vec{p}_\nu),$$
$$\epsilon_V(L) = \frac{1}{m_V}(p_V,0,0,E_V), \qquad \epsilon_V(\pm) = \frac{1}{\sqrt{2}}(0,\mp1,-i,0), \tag{31}$$

where M denotes the P and V meson, θ_ℓ is the polar angle of a neutrino with respect to the moving direction of the M meson in the q^2 rest frame, and the components of $\vec{p}_\ell$ can be obtained from $\vec{p}_\nu$ by using $\pi-\theta_\ell$ and $\phi+\pi$ instead of θ_ℓ and ϕ.

The solutions of the Dirac equation for positive and negative energy can be expressed, respectively, as

$$u_\pm(p) = \frac{1}{\sqrt{E+m}}\begin{pmatrix}\sqrt{E+m}\chi_\pm(\vec{p})\\ \vec{\sigma}\cdot\vec{p}\chi_\pm(\vec{p})\end{pmatrix},$$
$$v_\pm(p) = \frac{1}{\sqrt{E+m}}\begin{pmatrix}\vec{\sigma}\cdot\vec{p}\chi_\mp(\vec{p})\\ \sqrt{E+m}\chi_\mp(\vec{p})\end{pmatrix}, \tag{32}$$

where the $\pm$ indices in χ are the eigenvalues of $\vec{\sigma}\cdot\vec{p}/|\vec{p}|$ and $+$ $(-)$ denotes the left- (right-)handed state. If the spatial momentum of a particle is taken as $\vec{p} = p(\sin\theta\cos\phi, \sin\theta\sin\phi, \cos\theta)$, the eigenstates of $\vec{\sigma}\cdot\vec{p}$ can be found as

$$\chi_+(\vec{p}) = \begin{pmatrix}\cos\frac{\theta}{2}\\ e^{i\phi}\sin\frac{\theta}{2}\end{pmatrix}, \quad \chi_-(\vec{p}) = \begin{pmatrix}\sin\frac{\theta}{2}\\ -e^{i\phi}\cos\frac{\theta}{2}\end{pmatrix}. \tag{33}$$

With the Pauli-Dirac representation of γ matrices, which are defined as

$$\gamma^0 = \begin{pmatrix}\mathbf{1} & 0\\ 0 & -\mathbf{1}\end{pmatrix}, \quad \gamma^i = \begin{pmatrix}0 & \sigma^i\\ -\sigma^i & 0\end{pmatrix}, \quad \gamma_5 = \gamma^5 = \begin{pmatrix}0 & \mathbf{1}\\ \mathbf{1} & 0\end{pmatrix}, \tag{34}$$

we get $\bar{\ell}_{u_\pm}[\cdots](1-\gamma_5)\nu_{v_+} = 2\bar{\ell}_{u_\pm}[\cdots]\nu_{v_+}$, where $[\cdots] = \{1, \gamma^\mu, \sigma^{\mu\nu}\}$ and $\ell_{u_\pm}$ denote the charged lepton in $u_\pm$ states. Since we take neutrinos as massless particles, the neutrino states are always left-handed, i.e., $\bar{\ell}_{u_\pm}[\cdots](1-\gamma_5)\nu_{v_-} = 0$.

With the chosen coordinates and the spinors in Eqs. (32) and (33), the leptonic current in the lepton helicity basis for the $\bar{B} \to P\ell\bar{\nu}$ decay can be derived as

$$\begin{aligned}\bar{\ell}_{h=+}\not{\epsilon}_X(1-\gamma_5)\nu &= 2m_\ell\beta_\ell\cos\theta_\ell,\\ \bar{\ell}_{h=+}(1-\gamma_5)\nu &= -2\sqrt{q^2}\beta_\ell,\\ \bar{\ell}_{h=-}\not{\epsilon}_X(1-\gamma_5)\nu &= -2\sqrt{q^2}\beta_\ell\sin\theta_\ell,\\ \bar{\ell}_{h=-}(1-\gamma_5)\nu &= 0,\end{aligned} \tag{35}$$

where $\beta_\ell = \sqrt{1-m_\ell^2/q^2}$, and the auxiliary polarization vector e_X is defined as

$$|\vec{P}|e_X^\mu \equiv P^\mu - \frac{P\cdot q}{q^2}q^\mu, \qquad \epsilon_X^\mu\epsilon_{X\mu} = -1, \qquad |\vec{P}| = \sqrt{\frac{\lambda_P}{q^2}}.$$

In order to include the V-meson polarizations in the $\bar{B} \to V\ell\bar{\nu}$ decay, we separate a lepton current in the lepton helicity basis into longitudinal and transverse parts, where the longitudinal part of the V meson is given as

$$\bar{\ell}_{h=+}\not{\epsilon}_Z(1-\gamma_5)\nu = 2m_\ell\beta_\ell\cos\theta_\ell, \tag{36}$$

$$\bar{\ell}_{h=-}\not{\epsilon}_Z(1-\gamma_5)\nu = -2\sqrt{q^2}\beta_\ell\sin\theta_\ell, \tag{37}$$

while the two transverse parts of the V meson are, respectively, given as

$$\bar{\ell}_{h=+}\not{\epsilon}_V(T)(1-\gamma_5)\nu = -2m_\ell\beta_\ell\begin{cases}\frac{i}{\sqrt{2}}\sin\theta_\ell e^{-i\phi}\ (T=+),\\ \frac{i}{\sqrt{2}}\sin\theta_\ell e^{i\phi}\ (T=-),\end{cases} \tag{38}$$

$$\begin{aligned}&\bar{\ell}_{h=-}\not{\epsilon}_V(T)(1-\gamma_5)\nu\\ &\quad = -2\sqrt{q^2}\beta_\ell\begin{cases}\frac{-i}{\sqrt{2}}(1-\cos\theta_\ell)e^{-i\phi}\ (T=+),\\ \frac{i}{\sqrt{2}}(1+\cos\theta_\ell)e^{i\phi}\ (T=-).\end{cases}\end{aligned} \tag{39}$$

The auxiliary polarizations e_Z and $e_V(T)$ are defined, respectively, as

$$\frac{E_V}{m_V}e_Z^\mu \equiv \epsilon_V^\mu(L) - \frac{\epsilon\cdot q}{q^2}q^\mu, \quad \sqrt{\frac{\lambda_V}{2}}e_V^\mu(T) \equiv \varepsilon^{\mu\nu\rho\sigma}\epsilon_{V\nu}(T)P_\rho q_\sigma.$$

Using the helicity basis and the lepton currents discussed before, the $\bar{B} \to P\ell\bar{\nu}$ decay amplitudes with the charged lepton positive and negative helicity are, respectively, obtained as

$$\mathcal{M}_P^{h=+} = \frac{G_F V_{qb}}{\sqrt{2}}\left(2m_\ell\beta_\ell\frac{\sqrt{\lambda_P}}{\sqrt{q^2}}f_1^{BP}\cos\theta_\ell - 2\beta_\ell\sqrt{q^2}X_P^{0\ell}\right), \tag{40}$$

$$\mathcal{M}_P^{h=-} = \frac{G_F V_{qb}}{\sqrt{2}}(-2\beta_\ell\sqrt{\lambda_P}f_1^{BP}\sin\theta_\ell), \tag{41}$$

$$X_P^{0\ell} = \frac{m_B^2 - m_P^2}{q^2}m_\ell f_0^{BP} + (m_B + m_P)(C_{qb}^{R,\ell} + C_{qb}^{L,\ell})f_S^{BP}. \tag{42}$$

As mentioned earlier, since the V meson carries spin degrees of freedom, we separate each lepton helicity amplitude into longitudinal (L) and transverse (T) parts to show the V-meson polarization effects. Therefore, we write the helicity amplitudes of $\bar{B} \to V\ell\bar{\nu}$ for the longitudinal polarization of the V meson as

$$\mathcal{M}_V^{L,h=+} = -i\frac{G_F V_{qb}}{\sqrt{2}}\left(2m_\ell\beta_\ell h_V^0\cos\theta_\ell - 2\beta_\ell\frac{\sqrt{\lambda_V}}{\sqrt{q^2}}X_V^{0\ell}\right), \tag{43}$$

$$\mathcal{M}_V^{L,h=-} = -i\frac{G_F V_{qb}}{\sqrt{2}}\left(-2\sqrt{q^2}\beta_\ell h_V^0\sin\theta_\ell\right), \tag{44}$$

$$h_V^0(q^2) = \frac{1}{2m_V\sqrt{q^2}}\left[(m_B^2 - m_V^2 - q^2)(m_B + m_V)A_1^{BV} - \frac{\lambda_V}{m_B + m_V}A_2^{BV}\right],$$
$$X_V^{0\ell} = m_\ell A_0^{BV} + \frac{q^2}{2m_V}(C_{qb}^{R,\ell} - C_{qb}^{L,\ell})f_P^{BV}. \quad (45)$$

It can be seen that the formulas for $\mathcal{M}_V^{L,h=\pm}$ are similar to those for $\mathcal{M}_P^{h=\pm}$. The helicity amplitudes for the transverse polarizations of the V meson can be derived as

$$\mathcal{M}_V^{T=\pm,h=+} = i\frac{G_F V_{qb}}{\sqrt{2}}[-\sqrt{2}m_\ell\beta_\ell \sin\theta_\ell e^{\mp i\phi}]h_V^\pm, \quad (46)$$

$$\mathcal{M}_V^{T=\pm,h=-} = \mp i\frac{G_F V_{qb}}{\sqrt{2}}[-\sqrt{2}\sqrt{q^2}\beta_\ell(1 \mp \cos\theta_\ell)e^{\mp i\phi}]h_V^\pm,$$
$$h_V^\pm = \frac{\sqrt{\lambda_V}}{m_B + m_V}V^{BV} \mp (m_B + m_V)A_1^{BV}. \quad (47)$$

Since the charged Higgs boson affects only the longitudinal part, $\mathcal{M}_V^{T=\pm,h=\pm}$ are dictated by the SM. From these obtained helicity amplitudes, it can be seen that, due to angular-momentum conservation, $\mathcal{M}_P^{h=+}$ and $\mathcal{M}_V^{L(T),h=+}$, which come from $\bar{\ell}\gamma_\mu(1-\gamma_5)\nu$, are chirality suppressed and proportional to m_ℓ. However, the charged lepton in $\bar{\ell}(1-\gamma_5)\nu$, which arises from the charged Higgs interaction, prefers the $h = +$ state, and the associated contribution, in principle, exhibits no chiral suppression factor. Nevertheless, the m_ℓ factor indeed exists in our case due to the Cheng-Sher ansatz.

2. Angular differential decay rate, lepton helicity asymmetry, and forward-backward asymmetry

When the three-body phase space is included, the differential decay rates with lepton helicity and V polarization as a function of q^2 and $\cos\theta_\ell$ can be obtained as

$$\frac{d\Gamma_{P\ell}^{h=\pm}}{dq^2 d\cos\theta_\ell} = \frac{\sqrt{\lambda_P}}{512\pi^3 m_B^3}\beta_\ell^2|\mathcal{M}_P^{h=\pm}|^2,$$
$$\frac{d\Gamma_{V\ell}^{L(T),h=\pm}}{dq^2 d\cos\theta_\ell} = \frac{\sqrt{\lambda_V}}{512\pi^3 m_B^3}\beta_\ell^2|\mathcal{M}_V^{L(T),h=\pm}|^2. \quad (48)$$

Using Eq. (48), we can investigate various interesting physical quantities, such as the BR, lepton-helicity asymmetry, lepton forward-backward asymmetry (FBA), and polarization distributions of the V meson. We thus introduce these observables in the following discussions.

When the polar angle is integrated out, the differential decay rate with each lepton helicity as a function of q^2 can be obtained as follows: For the $\bar{B} \to P\ell\bar{\nu}$ decay, they can be expressed as

$$\frac{d\Gamma_{P\ell}^{h=\pm}}{dq^2} = \frac{G_F^2|V_{qb}|^2\sqrt{\lambda_P}\beta_\ell^4}{256\pi^3 m_B^3}H_P^\pm,$$
$$H_P^+ = \frac{2m_\ell^2}{3q^2}\lambda_P(f_1^{BP})^2 + 2q^2|X_P^{0\ell}|^2,$$
$$H_P^- = \frac{4}{3}\lambda_P(f_1^{BP})^2; \quad (49)$$

and for the $\bar{B} \to V\ell\nu$ decay, they are shown as

$$\frac{d\Gamma_{V\ell}^{\lambda,h=\pm}}{dq^2} = \frac{G_F^2|V_{qb}|^2\sqrt{\lambda_V}\beta_\ell^4}{256\pi^3 m_B^3}H_V^{\lambda,\pm},$$
$$H_V^{L,+} = \frac{2m_\ell^2}{3}|h_V^0|^2 + \frac{2\lambda_V}{q^2}|X_V^{0\ell}|^2,$$
$$H_V^{L,-} = \frac{4q^2}{3}|h_V^0|^2,$$
$$H_V^{T=\pm,+} = \frac{2m_\ell^2}{3}|h_V^\pm|^2,$$
$$H_V^{T=\pm,-} = \frac{4q^2}{3}|h_V^\pm|^2. \quad (50)$$

Accordingly, the partial decay rates for $\bar{B} \to (P,V)\ell\bar{\nu}$ can be directly obtained as

$$\Gamma_{P\ell} = \frac{G_F^2|V_{qb}|^2}{256\pi^3 m_B^3}\int_{m_\ell^2}^{q^2_{\max}} dq^2\sqrt{\lambda_P}\beta_\ell^4(H_P^+ + H_P^-),$$
$$\Gamma_{V\ell} = \frac{G_F^2|V_{qb}|^2}{256\pi^3 m_B^3}\int_{m_\ell^2}^{q^2_{\max}} dq^2\sqrt{\lambda_V}\beta_\ell^4\sum_{\lambda=L,T=\pm}(H_V^{\lambda,+} + H_V^{\lambda,-}). \quad (51)$$

Moreover, the q^2-dependent longitudinal polarization and transverse polarization fractions can be defined, respectively, as

$$f_{V\ell}^L(q^2) = \frac{\sum_h d\Gamma_{V\ell}^{L,h}/dq^2}{\sum_{\lambda,h}d\Gamma_{V\ell}^{\lambda,h}/dq^2} = \frac{H_V^{L,+} + H_V^{L,-}}{\sum_{\lambda,h}H_V^{\lambda,h}}, \quad (52)$$

$$f_{V\ell}^T(q^2) = \frac{\sum_{T,h}d\Gamma_{V\ell}^{T,h}/dq^2}{\sum_{\lambda,h}d\Gamma_{V\ell}^{\lambda,h}/dq^2} = \frac{\sum_{T=\pm}(H_V^{T,+} + H_V^{T,-})}{\sum_{\lambda,h}H_V^{\lambda,h}}. \quad (53)$$

Based on Eqs. (49) and (50), we define the q^2-dependent lepton helicity asymmetry as

$$\mathcal{P}_M^\ell(q^2) = \frac{d\Gamma_{M\ell}^{h=+}/dq^2 - d\Gamma_{M\ell}^{h=-}/q^2}{d\Gamma_{M\ell}^{h=+}/dq^2 + d\Gamma_{M\ell}^{h=-}/dq^2}, \quad (54)$$

where the sum of V polarizations is indicated in $d\Gamma_{V\ell}^{h=\pm}$. Thus, the results for the pseudoscalar and vector meson processes can be, respectively, formulated as

$$\mathcal{P}_P^{\ell}(q^2) = \frac{\frac{2}{3}(m_\ell^2 - 2q^2)\lambda_P (f_1^{BP})^2/q^2 + 2q^2|X_P^{0\ell}|^2}{\frac{2}{3}(m_\ell^2 + 2q^2)\lambda_P (f_1^{BP})^2/q^2 + 2q^2|X_P^{0\ell}|^2}, \tag{55}$$

$$\mathcal{P}_V^{\ell}(q^2) = \frac{\frac{2}{3}(m_\ell^2 - 2q^2)(\sum_{\lambda=L,\pm}|h_V^\lambda|^2) + 2\lambda_V/q^2|X_V^{0\ell}|^2}{\frac{2}{3}(m_\ell^2 + 2q^2)(\sum_{\lambda=L,\pm}|h_V^\lambda|^2) + 2\lambda_V/q^2|X_V^{0\ell}|^2}. \tag{56}$$

In addition, using the helicity decay rates, the q^2-independent lepton helicity asymmetry can be defined as [24,27,53,92,93]

$$P_M^{\ell} = \frac{\Gamma_{M\ell}^{h=+} - \Gamma_{M\ell}^{h=-}}{\Gamma_{M\ell}^{h=+} + \Gamma_{M\ell}^{h=-}}, \tag{57}$$

where the formulations for $\bar{B} \to (P, V)\ell\bar{\nu}$ with charged Higgs boson effects can be found as

$$P_P^{\ell} = \frac{\int_{m_\ell^2}^{q^2_{\max}} dq^2 \sqrt{\lambda_P}\beta_\ell^4 [\frac{2}{3}(m_\ell^2 - 2q^2)\lambda_P (f_1^{BP})^2/q^2 + 2q^2|X_P^{0\ell}|^2]}{\int_{m_\ell^2}^{q^2_{\max}} dq^2 \sqrt{\lambda_P}\beta_\ell^4 [\frac{2}{3}(m_\ell^2 + 2q^2)\lambda_P (f_1^{BP})^2/q^2 + 2q^2|X_P^{0\ell}|^2]}, \tag{58}$$

$$P_V^{\ell} = \frac{\int_{m_\ell^2}^{q^2_{\max}} dq^2 \sqrt{\lambda_V}\beta_\ell^4 [\frac{2}{3}(m_\ell^2 - 2q^2)(\sum_{\lambda=L,\pm}|h_V^\lambda|^2) + 2\lambda_V/q^2|X_V^{0\ell}|^2]}{\int_{m_\ell^2}^{q^2_{\max}} dq^2 \sqrt{\lambda_V}\beta_\ell^4 [\frac{2}{3}(m_\ell^2 + 2q^2)(\sum_{\lambda=L,\pm}|h_V^\lambda|^2) + 2\lambda_V/q^2|X_V^{0\ell}|^2]}. \tag{59}$$

From the angular differential decay rates shown in Eq. (48), the lepton FBA can be defined as

$$A_{FB}^{M,\ell}(q^2) = \frac{\int_0^1 dz(d\Gamma_{M\ell}/dq^2dz) - \int_{-1}^0 dz(d\Gamma_{M\ell}/dq^2dz)}{\int_0^1 dz(d\Gamma_{M\ell}/dq^2dz) + \int_{-1}^0 dz(d\Gamma_{M\ell}/dq^2dz)}, \tag{60}$$

where $z = \cos\theta_\ell$ and $d\Gamma_{M\ell}/(dq^2dz)$ have included all possible lepton helicities and polarizations of the V meson. The FBAs mediated by the charged Higgs boson and W boson in $\bar{B} \to (P, V)\ell\bar{\nu}_\ell$ are obtained as

$$\begin{aligned} A_{FB}^{P,\ell}(q^2) &= -\frac{2m_\ell\sqrt{\lambda_P} f_1^{BP}\mathrm{Re}(X_P^{0\ell *})}{H_P^+ + H_P^-}, \\ A_{FB}^{V,\ell}(q^2) &= \frac{1}{\sum_{\lambda=L,\pm}(H_V^{\lambda,+} + H_V^{\lambda,-})}\left[-2m_\ell\frac{\sqrt{\lambda_V}}{\sqrt{q^2}}\mathrm{Re}(h_V^0 X_V^{0\ell *})\right. \\ &\quad \left. + 4q^2\sqrt{\lambda_V}A_1^{BV}V^{BV}\right]. \end{aligned} \tag{61}$$

From the above equations, it can be seen that $A_{FB}^{P,\ell}$ and the longitudinal part of $A_{FB}^{V,\ell}$ depend on m_ℓ and are chiral suppressed. Since $m_\tau/m_b \sim 0.4$ is not highly suppressed, it can be expected that $\bar{B} \to P\tau\bar{\nu}$ can have a sizable FBA. $A_{FB}^{V,\ell}$ does not vanish in the chiral limit; therefore, it can be sizable for a light lepton.

The observations of the tau polarization and FBA rely on tau-lepton reconstruction. Because of the involvement of one invisible neutrino in the final state, it is experimentally challenging to measure these observables. As an alternative to the τ reconstruction, the extraction of τ polarization and FBA through an angular asymmetry of visible particles in a tau decay was recently proposed in Refs. [94,95], where the $\tau \to \pi\nu_\tau$ decay is the most sensitive channel. Using this approach, a statistical precision of 10% can be reached at Belle II with an integrated luminosity of 50 ab^{-1}. The detailed study can be found in Ref. [95].

IV. $\Delta B = 2$ AND $b \to s\gamma$ PROCESSES IN THE GENERIC 2HDM

It is known that tree-level FCNCs can occur in the generic 2HDM; therefore, the measured mass difference $\Delta M_{q'}$ ($q' = d, s$) of a neutral $B_{q'}$ meson will give a strict limit on the parameters $X^d_{q'b,bq'}$. In our approach, due to the Cheng-Sher ansatz, the $\Delta B = 2$ process, mediated by the neutral scalars at the tree level, is proportional to $m_{q'}m_b t_\beta^2/v^2(\chi^d_{q'b})^2$. Although the tree-level effect has a suppression factor $m_{q'}/v$, the factor t_β^2 can largely enhance its contribution; hence, $\Delta M_{q'}$ will severely bound the $\chi^d_{q'b,bq'}$ parameters.

In addition to the tree-level effects, we find through box diagrams that the charged Higgs boson contributions to $\Delta B = 2$ can be significant when t_β is large, and $\chi^u_{tt,ct}$ and χ^d_{bb} are of $O(0.1)$–$O(1)$. The same charged Higgs boson effects also contribute to the radiative $b \to s(d)\gamma$ decay via penguin diagrams. Since $b \to s\gamma$ is measured well in experiments, in this study, we focus only on the $b \to s\gamma$ decay. It is of interest to investigate whether the sizable new parameters $\chi^u_{tt,ct}$ and χ^d_{bb} in the generic 2HDM can accommodate the $\Delta M_{q'}$ and $b \to s\gamma$ data. Hence, in this section, we formulate the contributions of the charged Higgs boson and neutral Higgs bosons to the $B_{d,s}$-$\bar{B}_{d,s}$ mixings and $b \to s\gamma$ process.

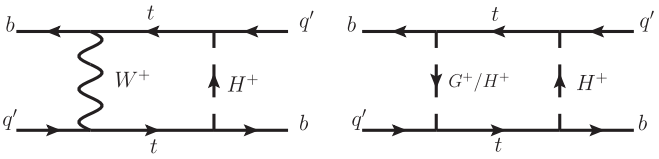

FIG. 1. The representative box diagrams for the $B_{q'}$-$\bar{B}_{q'}$ mixing with the intermediates of W^+-H^+, G^+-H^+, and H^+-H^+, where G^+ is the charged Goldstone boson.

A. Charged Higgs boson contributions to the $\Delta M_{q'}$

We first consider the charged Higgs boson contributions to the $\Delta B = 2$ processes, where the typical Feynman diagrams mediated by W^+-H^+, G^+-H^+, and H^+-H^+ are sketched in Fig. 1 and G^+ is the charged Goldstone boson. Since the Yukawa couplings of $H^\pm$ to the quarks are associated with the quark masses, the vertices that involve heavy quarks can enhance the loop $H^\pm$ effects. Thus, we consider only the top-quark loop contributions in the B-meson system. Accordingly, the relevant charged Higgs interactions are shown as

$$\mathcal{L}_Y^{H^\pm} \supset \frac{\sqrt{2}}{v} V_{tb}\bar{t}(m_t\zeta^u_{tt}P_L + m_b\zeta^d_{bb}P_R)bH^+ + \frac{\sqrt{2}}{v} V_{tq'}\bar{t}(m_t\zeta^u_{tq'}P_L - m_b\zeta^d_{tq'}P_R)q'H^+ + \text{H.c.}, \tag{62}$$

where the parameters ζ^f_{ij} are defined as

$$\zeta^u_{tt} \approx \frac{1}{t_\beta} - \frac{\chi^{u*}_{tt}}{s_\beta}, \qquad \zeta^d_{bb} \approx t_\beta\left(1 - \frac{\chi^d_{bb}}{s_\beta}\right),$$
$$\zeta^u_{tq'} \approx \frac{1}{t_\beta} - \frac{\chi^L_{tq'}}{s_\beta}, \qquad \zeta^d_{tq'} = t_\beta\left(\sqrt{\frac{m_{q'}}{m_b}}\frac{\chi^d_{bq'}}{s_\beta}\frac{V_{tb}}{V_{tq'}}\right),$$
$$\chi^L_{tq'} = \chi^{u*}_{tt} + \sqrt{\frac{m_c}{m_t}}\frac{V_{cq'}}{V_{tq'}}\chi^{u*}_{ct}. \tag{63}$$

Detailed discussions for the couplings of $tq'H^\pm$ can be found in the Appendix. From Eqs. (62) and (63), when $\chi^f_{ij} = 0$, the vertices in the type-II 2HDM are reproduced. Unlike the type-II model, where $\zeta^u_{tt,tq'} \ll 1$ for $t_\beta \sim m_t/m_b$, $\zeta^u_{tt,tq'}$ in the type-III model can be of the order of unity even at small t_β. We will show the impacts of these new 2HDM parameters on the flavor physics in the following analysis.

Based on the convention in Ref. [96], the effective Hamiltonian for $B_{q'}$-$\bar{B}_{q'}$ mixing can be written as

$$H^{\Delta B=2}_{\text{eff}} = \frac{G_F^2(V^*_{tb}V_{tq'})^2}{16\pi^2}m_W^2\left(\sum_{i=1}^{5}C_i(\mu)Q_i + \sum_{i=1}^{3}\tilde{C}_i(\mu)\tilde{Q}_i\right), \tag{64}$$

where the effective operators with the color indices α and β are given as

$$Q_1 = (\bar{b}^\alpha\gamma_\mu P_L q'^\alpha)(\bar{b}^\beta\gamma^\mu P_L q'^\beta),$$
$$Q_2 = (\bar{b}^\alpha P_L q'^\alpha)(\bar{b}^\beta P_L q'^\beta),$$
$$Q_3 = (\bar{b}^\beta P_L q'^\alpha)(\bar{b}^\alpha P_L q'^\beta),$$
$$Q_4 = (\bar{b}^\alpha P_L q'^\alpha)(\bar{b}^\beta P_R q'^\beta),$$
$$Q_5 = (\bar{b}^\beta P_L q'^\alpha)(\bar{b}^\alpha P_R q'^\beta). \tag{65}$$

The operators $\tilde{O}_j$ can be obtained from O_j using P_R instead of P_L. The Wilson coefficients at the scale $\mu = m_b = 4.6$ GeV can be related to those at μ_H scale and are given as [96]

$$C_i(m_b) \approx \sum_{k,j}(b^{(i,j)}_k + \eta c^{(i,j)}_k)\eta^{a_k}C_j(\mu_H), \tag{66}$$

where $\mu_H = m_{H^\pm}$, $\eta = \alpha_s(\mu_H)/\alpha_s(m_t)$, $C_j(\mu_H)$ are the Wilson coefficients at the μ_H scale, and the magic numbers for a_k, $b^{(i,j)}_k$, and $c^{(i,j)}_k$ can be found in Ref. [96]. To obtain $C_j(\mu_H)$, we adopt the 't Hooft–Feynman gauge for the propagator of the W-gauge boson; therefore, the charged Goldstone $G^\pm$ boson effects have to be taken into account. To show the results of the box diagrams, we define some useful parameters as $x_t = m_t^2/m_W^2$, $y_t = m_t^2/m_{H^\pm}^2$, $y_W = m_W^2/m_{H^\pm}^2$, and $y_b = m_b^2/m_{H^\pm}^2$. Thus, the effective Wilson coefficients at the μ_H scale can be formulated as

$$C_1(\mu_H) = 4\zeta^u_{tq'}\zeta^{u*}_{tt}(2y_t^2 I_1^{WH}(y_t, y_W) + x_t y_t I_2^{WH}(y_t, y_W)) + 2(\zeta^u_{tq'}\zeta^{u*}_{tt})^2 x_t y_t I_1^{HH}(y_t), \tag{67a}$$

$$C_2(\mu_H) = -4(\zeta^u_{tq'}\zeta^{d*}_{bb})^2 x_b y_t^2 I_2^{HH}(y_t), \tag{67b}$$

TABLE I. Values of quark masses, B_{iq} parameters, and $\hat{\eta}_{iB}$ at the m_b scale in the regularization-independence momentum subtraction scheme, where the B_{iq} results are quoted from Ref. [104]. The decay constants of the $B_{d,s}$ mesons are from Ref. [106], and f_{B_c} is from Ref. [107].

m_b	m_s	$m_{q'}$	f_{B_s}	f_{B_d}	f_{B_c}	$B_{1q'}$	$B_{2q'}$	$B_{3q'}$
4.6 GeV	0.10 GeV	5.4 MeV	0.231 GeV	0.191 GeV	0.434 GeV	0.84	0.88	1.10
$B_{4q'}$	$B_{5q'}$	$\hat{\eta}_{1B}$	$\hat{\eta}_{2B}$	$\hat{\eta}_{3B}$	$\hat{\eta}_{44B}$	$\hat{\eta}_{45B}$	$\hat{\eta}_{54B}$	$\hat{\eta}_{55B}$
1.12	1.89	0.848	1.708	−0.016	2.395	0.061	0.431	0.094

$$C_4(\mu_H) = 8\frac{m_b^2}{m_t^2}\zeta^d_{tq'}\zeta^{d*}_{bb}(2y_t I_2^{WH}(y_t,y_W) + x_t y_t^2 I_1^{WH}(y_t,y_W)) + 8(\zeta^d_{tq'}\zeta^{u*}_{tt})(\zeta^u_{tq'}\zeta^{d*}_{bb})x_b y_t^2 I_2^{HH}(y_t), \quad (67c)$$

$$C_5(\mu_H) = -8(\zeta^u_{tq'}\zeta^{u*}_{tt})(\zeta^d_{tq'}\zeta^{d*}_{bb})x_b y_t I_1^{HH}(y_t), \quad (67d)$$

where the loop integral functions are defined as

$$I_1^{WH}(y_t,y_W) = \int_0^1 dx_1 \int_0^{x_1} dx_2 \frac{x_2}{(1-x_1+y_t x_2 + y_W(x_1-x_2))^2}, \quad (68a)$$

$$I_2^{WH}(y_t,y_W) = \int_0^1 dx_1 \int_0^{x_1} dx_2 \frac{x_2}{1-x_1+y_t x_2 + y_W(x_1-x_2)}, \quad (68b)$$

$$I_1^{HH}(y_t) = \int_0^1 dx \frac{x(1-x)}{1-x+y_t x}, \quad (68c)$$

$$I_2^{HH}(y_t) = \int_0^1 dx \frac{x(1-x)}{(1-x+y_t x)^2}. \quad (68d)$$

The effective Wilson coefficients for the $\tilde{O}_{1,2}$ operators at μ_H scale are given as

$$\tilde{C}_1(\mu_H) = 2(\zeta^d_{tq'}\zeta^{d*}_{bb})^2 x_b y_b I_1^{HH}(y_t),$$
$$\tilde{C}_2(\mu_H) = -4(\zeta^d_{tq'}\zeta^{u*}_{tt})^2 x_b y_t^2 I_2^{HH}(y_t). \quad (69)$$

We have checked that our results are the same as those obtained in Ref. [97] when $y_b = \chi^{u,d}_{ij} = 0$. Using Eq. (66) and the magic numbers shown in Ref. [96], we obtain the Wilson coefficients $C_i(m_b)$ at the $\mu = m_b$ scale as

$$C_1(m_b) \approx 0.848 C_1(\mu_H),$$
$$C_2(m_b) \approx 1.708 C_2(\mu_H),$$
$$C_3(m_b) \approx -0.016 C_2(\mu_H),$$
$$C_4(m_b) \approx 2.395 C_4(\mu_H) + 0.431 C_5(\mu_H),$$
$$C_5(m_b) \approx 0.061 C_4(\mu_H) + 0.904 C_5(\mu_H). \quad (70)$$

The matrix elements of the renormalized operators for $\Delta B = 2$ are defined as [96]

$$\langle B_{q'}|\hat{Q}_1(\mu)|\bar{B}_{q'}\rangle = \frac{1}{3} f^2_{B_{q'}} m_{B_{q'}} B_{1q'}(\mu), \quad (71a)$$

$$\langle B_{q'}|\hat{Q}_2(\mu)|\bar{B}_{q'}\rangle = -\frac{5}{24}\left(\frac{m_{B_{q'}}}{m_b(\mu)+m_{q'}(\mu)}\right)^2 f^2_{B_q} m_{B_{q'}} B_{2q'}(\mu), \quad (71b)$$

$$\langle B_{q'}|\hat{Q}_3(\mu)|\bar{B}_{q'}\rangle = \frac{1}{24}\left(\frac{m_{B_{q'}}}{m_b(\mu)+m_{q'}(\mu)}\right)^2 f^2_{B_{q'}} m_{B_{q'}} B_{3q'}(\mu), \quad (71c)$$

$$\langle B_{q'}|\hat{Q}_4(\mu)|\bar{B}_{q'}\rangle = \frac{1}{4}\left(\frac{m_{B_{q'}}}{m_b(\mu)+m_{q'}(\mu)}\right)^2 f^2_{B_{q'}} m_{B_{q'}} B_{4q'}(\mu), \quad (71d)$$

$$\langle B_{q'}|\hat{Q}_5(\mu)|\bar{B}_{q'}\rangle = \frac{1}{12}\left(\frac{m_{B_{q'}}}{m_b(\mu)+m_{q'}(\mu)}\right)^2 f^2_{B_{q'}} m_{B_{q'}} B_{5q'}(\mu), \quad (71e)$$

where $B_{iq'}$ denote the nonperturbative QCD bag parameters and the mixing matrix elements in the SM are related to $B_{1q'}$. Using the results obtained by the HPQCD [98], FNAL-MILC [99], and RBC-UKQCD [100] Collaborations, the lattice QCD results with $N_f = 2+1$ averaged by the flavor lattice averaging group can be found as $B_{1d} \approx 0.80$ and $B_{1s} \approx 0.84$ [101]. In our numerical calculations, the quark masses and $B_{iq'}$ parameters at the m_b scale in the Landau regularization-independence momentum subtraction scheme [96,102–104] and the decay constants of $B_{q'}$ are shown in Table I, where, for self-consistency, all B_{iq} values are quoted from Ref. [104]. Because of $B_{is} \approx B_{id}$, we adopt $B_{is} = B_{id} \equiv B_{iq'}$. As a result, $\langle B_{q'}|H^{\Delta B=2}_{\rm eff}|\bar{B}_{q'}\rangle$ can be written as

$$\langle B_{q'}|H^{\Delta B=2}_{\rm eff}|\bar{B}_{q'}\rangle = \langle B_{q'}|H^{\Delta B=2}_{\rm eff}|\bar{B}_{q'}\rangle^{\rm SM}(1+\Delta^{H^\pm}_{q'}). \quad (72)$$

The SM result and the charged Higgs boson contributions can be formulated as

$$\langle B_{q'}|H^{\Delta B=2}_{\rm eff}|\bar{B}_{q'}\rangle^{\rm SM} = \frac{G_F^2(V^*_{tb}V_{tq'})^2}{48\pi^2} m_W^2 f^2_{B_{q'}} m_{B_{q'}} \hat{\eta}_{1B} B_{1q'}(4S_0(x_t)),$$
$$\Delta^{H^\pm}_{q'} = \frac{1}{4S_0(x_t)}\Big\{C_1(\mu_H) + \tilde{C}_1(\mu_H) + \frac{m^2_{B_{q'}}}{8(m_b+m_{q'})^2\hat{\eta}_{1B}B_{1q'}}[(-5\hat{\eta}_{2B}B_{2q'} + \hat{\eta}_{3B}B_{3q'})(C_2(\mu_H)+\tilde{C}_2(\mu_H)) + (6\hat{\eta}_{44B}B_{4q'} + 2\hat{\eta}_{45B}B_{5q'})C_4(\mu_H) + (6\hat{\eta}_{54B}B_{4q'} + 2\hat{\eta}_{55B}B_{5q'})C_5(\mu_H)]\Big\}, \quad (73)$$

where $4S_0(m_t^2/m_W^2) = 3.136(m_t^2/m_W^2)^{0.76} \approx 9.36$ [105]; $\hat{\eta}_{iB}$ are the QCD corrections, and their values are shown in Table I. Accordingly, the mass difference between the physical $B_{q'}$ states can be obtained by

$$\Delta M_{q'}^{H^\pm} = 2|\langle B_{q'}|H_{\rm eff}^{\Delta B=2}|\bar{B}_{q'}\rangle| = \Delta M_{q'}^{\rm SM}|1+\Delta_{q'}^{H^\pm}|. \quad (74)$$

Taking $V_{td} \approx 0.0082e^{-i\phi_1}$ with $\phi_1 \approx 21.9°$, $V_{ts} \approx -0.04$, and $m_t = \bar{m}_t(\bar{m}_t) \approx 165$ GeV, the $B_{q'}$-meson oscillation parameters $\Delta M_{d,s}$ in the SM are, respectively, estimated as

$$\Delta M_d^{\rm SM} \approx 3.20\times 10^{-13}\ {\rm GeV} = 0.487\ {\rm ps}^{-1},$$
$$\Delta M_s^{\rm SM} \approx 1.13\times 10^{-11}\ {\rm GeV} = 17.22\ {\rm ps}^{-1}, \quad (75)$$

where the current data are $\Delta M_d^{\rm exp} = (0.5065 \pm 0.0019)\ {\rm ps}^{-1}$ and $\Delta M_s^{\rm exp} = (17.756 \pm 0.021)\ {\rm ps}^{-1}$ [70]. In order to include the new physics contributions, when we use the $\Delta M_{q'}^{\rm exp}$ to bound the free parameters, we take the SM predictions to be $\Delta M_d^{\rm SM} = 0.555^{+0.073}_{-0.046}\ {\rm ps}^{-1}$ and $\Delta M_s^{\rm SM} = 16.8^{+2.6}_{-1.5}\ {\rm ps}^{-1}$ [106], in which the next-to-leading-order (NLO) QCD corrections [108–110] and the uncertainties from various parameters, such as CKM matrix elements, decay constants, and the top-quark mass, are taken into account. Hence, from Eq. (74), the bounds from $\Delta B = 2$ can be used as

$$0.76 \lesssim |1+\Delta_d^{H^\pm}| \lesssim 1.15,$$
$$0.87 \lesssim |1+\Delta_s^{H^\pm}| \lesssim 1.38. \quad (76)$$

B. $\Delta M_{q'}$ from the tree FCNCs

To formulate the scalar boson contributions to $\Delta M_{q'}$ at the tree level, we write the Yukawa couplings of scalars H and A to the quarks with Cheng-Sher ansatz as [5]

$$-\mathcal{L}_Y^{H,A} = \frac{t_\beta}{v}\bar{d}_{iL}\left[m_{d_i}\delta_{ij} - \frac{\sqrt{m_{d_i}m_{d_j}}}{s_\beta}\chi_{ij}^d\right]d_{jR}(H-iA) + {\rm H.c.} \quad (77)$$

The effective Hamiltonian for the $\Delta B = 2$ process mediated by the neutral scalar bosons H and A at the μ_H scale can then be straightforwardly obtained as

$$\mathcal{H}_S^{\Delta B=2} = -\left(\frac{m_b t_\beta}{v s_\beta}\right)^2\frac{m_{q'}}{4m_b}\left[(\chi_{q'b}^{d*})^2\left(\frac{1}{m_H^2}-\frac{1}{m_A^2}\right)Q_2 + (\chi_{bq'}^{d})^2\left(\frac{1}{m_H^2}-\frac{1}{m_A^2}\right)\tilde{Q}_2 + 2\chi_{bq'}^{d}\chi_{q'b}^{d*}\left(\frac{1}{m_H^2}+\frac{1}{m_A^2}\right)Q_4\right]. \quad (78)$$

It can be seen that, when $m_H = m_A$, the contributions from the operators Q_2 and $\tilde{Q}_2$ vanish. We note that the box diagrams, mediated by Z-$H(A)$, G^0-$H(A)$, and $H(A)$-$H(A)$, involve the q_i-b-$H(A)$ FCNC couplings, which are the same as the tree contributions. Thus, it is expected that the box contributions will be smaller than the tree; therefore, we do not further discuss such box diagrams and neglect their contributions.

Using Eq. (66) and the hadronic matrix elements shown in Eq. (71), the $\Delta M_{q'}$, which combines the SM and $S = H + A$ effects, can be found as

$$\Delta M_{q'}^S = 2|\langle B_{q'}|H_S^{\Delta B=2}|\bar{B}_{q'}\rangle| = \Delta M_{q'}^{\rm SM}|1+\Delta_{q'}^S|, \quad (79)$$

where the H and A contributions are expressed as

$$\Delta_{q'}^S = -\frac{1}{4S_0(x_t)}\left(\frac{\sqrt{2}\pi^2 t_\beta^2\sqrt{x_b x_{q'}}}{2G_F(V_{tb}^*V_{tq'})^2 s_\beta}\right)\frac{m_{B_{q'}}^2}{(m_b+m_{q'})^2\hat{\eta}_{1B}B_{1q'}} \times[(-5\hat{\eta}_{2B}B_{2q'}+\hat{\eta}_{3B}B_{3q'})(C_2^S+\tilde{C}_2^S) + (6\hat{\eta}_{44B}B_{4q'}+2\hat{\eta}_{45B}B_{5q'})C_4^S]; \quad (80)$$

$x_{b(q')} = m_{b(q')}^2/m_W^2$, the $\hat{\eta}_{iB}$ are the QCD factors as shown in Table I, and the factors C_2^S, $\tilde{C}_2^S$, and C_4^S are defined, respectively, as

$$C_2^S = (\chi_{q'b}^{d*})^2\left(\frac{1}{m_H^2}-\frac{1}{m_A^2}\right),$$
$$\tilde{C}_2^S = (\chi_{bq'}^{d})^2\left(\frac{1}{m_H^2}-\frac{1}{m_A^2}\right),$$
$$C_4^S = 2\chi_{q'b}^{d*}\chi_{bq'}^{d}\left(\frac{1}{m_H^2}+\frac{1}{m_A^2}\right). \quad (81)$$

Since Eq. (79) is directly related to $\chi_{bq',q'b}^d$, in order to show the $\Delta M_{q'}$ constraint on the different parameters, here we do not combine the neutral scalar with the charged Higgs boson contributions. According to Eq. (76), the bounds on $\Delta_{d,s}^S$ can be given as

$$0.76 \lesssim |1+\Delta_d^S| \lesssim 1.15,$$
$$0.87 \lesssim |1+\Delta_s^S| \lesssim 1.38. \quad (82)$$

C. Charged Higgs boson contributions to the $b \to s\gamma$ process

In addition to the $\Delta B = 2$ processes, the penguin-induced $b \to s\gamma$ decay is also sensitive to new physics. The current experimental value is ${\rm BR}(\bar{B}\to X_s\gamma)^{\rm exp} = (3.32\pm0.15)\times10^{-4}$ for $E_\gamma > 1.6$ GeV [15], and the SM prediction with next-to-next-to-leading-order (NNLO) QCD corrections is ${\rm BR}(\bar{B}\to X_s\gamma)^{\rm SM} = (3.36\pm0.23)\times10^{-4}$ [111,112]. Since the SM result is

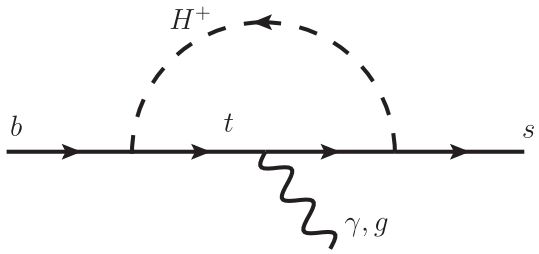

FIG. 2. Penguin diagrams for $b \to s(\gamma, g)$ with the intermediate of $H^\pm$.

close to the experimental data, we can use the $\bar{B} \to X_s\gamma$ decay to give a strict bound on the new physics effects. The effective Hamiltonian arisen from the $W^\pm$ and $H^\pm$ bosons for $b \to s\gamma$ at the μ_H scale can be written as

$$\mathcal{H}_{b\to s\gamma} = -\frac{4G_F}{\sqrt{2}} V_{ts}^* V_{tb} (C_{7\gamma}(\mu_H) Q_{7\gamma} + C_{8\gamma}(\mu_H) Q_{8G} + C'_{7\gamma}(\mu_H) Q'_{7\gamma} + C'_{8\gamma}(\mu_H) Q'_{8G}), \tag{83}$$

where the electromagnetic and gluonic dipole operators are given, respectively, as

$$Q_{7\gamma} = \frac{e}{16\pi^2} m_b \bar{s} \sigma^{\mu\nu} P_R b F_{\mu\nu},$$
$$Q_{8G} = \frac{g_s}{16\pi^2} m_b \bar{s}_\alpha \sigma^{\mu\nu} T^a_{\alpha\beta} P_R b_\beta G^a_{\mu\nu} \tag{84}$$

and the $Q'_{7\gamma,8G}$ operators can be obtained from the unprimed operator using P_L instead of P_R. We note that $C'_{7\gamma,8G}$ from the SM contributions are suppressed by m_s and are negligible; therefore, the main primed operators are from the new physics effects.

According to the charged Higgs interactions in Eq. (62), the relevant Feynman diagrams for $b \to s(\gamma, g)$ are sketched in Fig. 2, and the $H^\pm$ contributions to $C^{H^\pm}_{7\gamma,8G}$ at the μ_H scale can be derived as

$$C^{H^\pm}_{7\gamma(8G)}(\mu_H) = \zeta^{u*}_{ts}\zeta^u_{tt} C^{H^\pm}_{7(8),LL}(y_t) + \zeta^{u*}_{ts}\zeta^d_{bb} C^{H^\pm}_{7(8),RL}(y_t),$$
$$C'^{H^\pm}_{7\gamma(8G)}(\mu_H) = \zeta^{d*}_{ts}\zeta^d_{bb} C^{H^\pm}_{7(8),RR}(y_t) + \zeta^{d*}_{ts}\zeta^u_{tt} C^{H^\pm}_{7(8),LR}(y_t), \tag{85}$$

where the loop integral functions are defined as

$$C^{H^\pm}_{7,LL}(y_t) = \frac{y_t}{72}\left[\frac{8y_t^2 + 5y_t - 7}{(1-y_t)^3} - \frac{6y_t(2-3y_t)}{(1-y_t)^4}\ln(y_t)\right], \tag{86a}$$

$$C^{H^\pm}_{8,LL}(y_t) = \frac{y_t}{24}\left[\frac{y_t^2 - 5y_t - 2}{(1-y_t)^3} - \frac{6y_t}{(1-y_t)^4}\ln(y_t)\right], \tag{86b}$$

$$C^{H^\pm}_{7,RL}(y_t) = \frac{y_t}{12}\left[\frac{3-5y_t}{(1-y_t)^2} + \frac{2(2-3y_t)}{(1-y_t)^3}\ln(y_t)\right], \tag{86c}$$

$$C^{H^\pm}_{8,RL}(y_t) = \frac{y_t}{4}\left[\frac{3-y_t}{(1-y_t)^2} + \frac{2}{(1-y_t)^3}\ln(y_t)\right], \tag{86d}$$

$C'^{H^\pm}_{7(8),RR}(y_t) = -(m_b^2/m_t^2) C^{H^\pm}_{7(8),LL}(y_t)$, and $C'^{H^\pm}_{7(8),LR}(y_t) = -C^{H^\pm}_{7(8),RL}(y_t)$. From Eq. (85), we can easily understand the effects of the type-II 2HDM as follows: Taking $\chi^u_{tt,ct} = \chi^d_{bb,sb} = 0$ in Eq. (85), $(\zeta^{u*}_{ts}\zeta^u_{tt})_{\text{type-II}}$ is suppressed by $1/t_\beta^2$, and $(\zeta^u_{bb}\zeta^{u*}_{ts})_{\text{type-II}} = 1$ becomes t_β independence. As a result, the mass of charged Higgs boson in the type-II 2HDM is limited to be $m_{H^\pm} > 580$ GeV at 95% confidence level (C.L.) when NNLO QCD corrections are taken into account [75]. In the generic 2HDM, since the new parameters $\chi^u_{tt,ct}/c_\beta$ and χ^d_{bb}/s_β are involved in Eq. (85), we have more degrees of freedom to reduce $\zeta^u_{bb}\zeta^{u*}_{ts}$ away from unity; thus, the charged Higgs mass can be lighter than 580 GeV.

To calculate the BR of $\bar{B} \to X_s\gamma$, we employ the results in Refs. [113,114], which are shown as

$$\mathrm{BR}(\bar{B} \to X_s\gamma) = 2.47 \times 10^{-3}(|C_{7\gamma}(\mu_b)|^2 + |C'_{7\gamma}(\mu_b)|^2 + N(E_\gamma)), \tag{87}$$

where $N(E_\gamma) = (3.6 \pm 0.6) \times 10^{-3}$ denotes a nonperturbative effect; $C_{7\gamma}(\mu_b) = C^{\mathrm{SM}}_{7\gamma}(\mu_b) + C^{H^\pm}_{7\gamma}(\mu_b)$ and $C'_{7\gamma}(\mu_b) = C'^{H^\pm}_{7\gamma}(\mu_b)$ are the Wilson coefficients at the μ_b scale, and their relations to the initial conditions at the higher-energy scalar μ_H occur through renormalization group (RG) equations. Using Eq. (87) and $\mathrm{BR}(\bar{B} \to X_s\gamma)^{\mathrm{SM}} \approx 3.36 \times 10^{-4}$, we obtain $C^{\mathrm{SM}}_{7\gamma} \approx -0.364$ at $\mu_b \approx 2.5$ GeV. The NLO [115–117] and NNLO [118] QCD corrections to the $C_{7\gamma}(\mu_b)$ in the 2HDM have been calculated. In this study, the charged Higgs boson effects with RG running are taken from Refs. [113,114], and they are written as

$$C^{(\prime)H^\pm}_{7\gamma}(\mu_b) = \kappa_7 C^{(\prime)H^\pm}_{7\gamma}(\mu_H) + \kappa_8 C^{(\prime)H^\pm}_{8G}(\mu_H), \tag{88}$$

where $\kappa_{7,8}$ are the LO QCD effects, for which their values with different values of μ_H can be found in Refs. [113,114].

D. H/A contributions to the $b \to s\gamma$ process

In addition to the charged currents, the $b \to s\gamma$ process can be generated through the FCNCs in the type-III 2HDM, where the corresponding Feynman diagrams for $b \to s(\gamma, g)$ are shown in Fig. 3. From the diagrams, it can be seen that, unlike the $m_t^2/m_{H^\pm}^2$ result from the $H^\pm$ and top-quark loops, the b-quark loops are suppressed by $m_b^2/m_{H,A}^2$. Therefore, it is expected that the

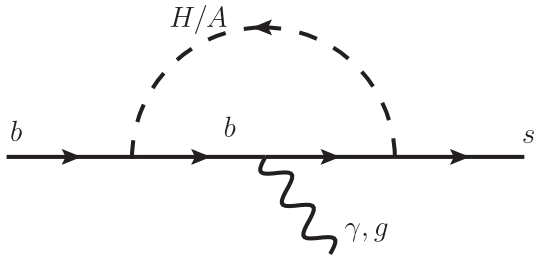

FIG. 3. The same as Fig. 2 but with the intermediates of neutral scalar bosons H and A.

radiative b decay induced by the neutral currents will be much smaller than the charged currents.

Using the Yukawa couplings in Eq. (77), we can derive the Wilson coefficients of $C_{7\gamma}$ and $C'_{7\gamma}$ at the μ_H scale, defined in Eq. (83), as

$$C^S_{7\gamma} = -\frac{t_\beta^2 Q_b}{4V^*_{ts}V_{tb}}\sqrt{\frac{m_s}{m_b}}\frac{\chi^d_{sb}}{s_\beta}\mathcal{N}_S,$$
$$C'^S_{7\gamma} = -\frac{t_\beta^2 Q_b}{4V^*_{ts}V_{tb}}\sqrt{\frac{m_s}{m_b}}\frac{\chi^{d*}_{bs}}{s_\beta}\mathcal{N}^*_S, \tag{89}$$

$$\mathcal{N}_S = -\left(1-\frac{\chi^{d*}_{bb}}{s_\beta}\right)\left[J_1\left(\frac{m_b^2}{m_A^2}\right)+J_1\left(\frac{m_b^2}{m_H^2}\right)\right] + \left(1-\frac{\chi^{d}_{bb}}{s_\beta}\right)\left[J_2\left(\frac{m_b^2}{m_A^2}\right)-J_2\left(\frac{m_b^2}{m_H^2}\right)\right], \tag{90}$$

where the superscript S denotes the scalar contributions; $Q_b = -1/3$ is the electric charge of b quark, and the functions $J_{1,2}$ are defined as

$$J_1(y) = \frac{y}{6}\left[\frac{1}{1-y}+\frac{y\ln(y)}{(1-y)^2}\right],$$
$$J_2(y) = \frac{y}{2}\left[-\frac{1}{1-y}+\frac{(y-2)\ln(y)}{(1-y)^2}\right]. \tag{91}$$

The contributions of H and A bosons to the chromomagnetic dipole operators can be related to the electromagnetic dipole operators, and the relations can be easily found as $C^{(\prime)S}_{8G} = C^{(\prime)S}_{7\gamma}/Q_b$. We can apply the result in Eq. (88) to get the Wilson coefficients at the μ_b scale as

$$C^{(\prime)S}_{7\gamma}(\mu_b) = \kappa_7 C^{(\prime)S}_{7\gamma}(\mu_H) + \kappa_8 C^{(\prime)S}_{8G}(\mu_H). \tag{92}$$

Using Eq. (87), we can directly obtain the S-mediated $\mathrm{BR}(\bar{B}\to X_s\gamma)$.

V. NUMERICAL ANALYSIS AND DISCUSSIONS

A. Numerical and theoretical inputs

In addition to the parameter values shown in Table I, the values of the CKM matrix elements used in the following analysis are taken as [15]

$$V_{ub} \approx 0.0037e^{-i\phi_3}, \quad \phi_3 = 73.5°,$$
$$V_{cd(s)} \approx -0.22(0.973), \quad V_{cb} \approx 0.0393,$$
$$V_{td} \approx 0.0082e^{-i\phi_1}, \quad \phi_1 = 21.9°,$$
$$V_{ts} \approx -0.040, \quad V_{tb} \approx 1.0. \tag{93}$$

To study the semileptonic $\bar{B}\to(P,V)\ell\bar{\nu}$ decays, we need the information for the $\bar{B}\to(P,V)$ transition form factors. For the $\bar{B}\to\pi$ decay, we use the results obtained by the LCSRs and express them as [68,69]

$$f_1^{B\pi}(q^2) = \frac{f_1(0)}{1-q^2/5.32^2}\left(1+\frac{r_{BZ}q^2/5.32^2}{1-\alpha_{BZ}q^2/m_B^2}\right),$$
$$f_0^{B\pi}(q^2) = \frac{f_1(0)}{1-q^2/33.81}, \tag{94}$$

where we take $f_1(0) = 0.245$, $\alpha_{BZ} = 0.40$, and $r_{BZ} = 0.64$. It is worth mentioning that lattice QCD results with $N_f = 2+1$ for the $\bar{B}\to\pi$ form factors, calculated by the HPQCD [119], FNAL-MILC [67], and RBC-UKQCD [120] Collaborations, recently have made significant progress. The detailed summary of the lattice QCD results can be found in Ref. [101]. We checked that the results of LCSRs are consistent with the values of Table IV in Ref. [120]. For the $\bar{B}\to\rho$ decay, the form factors based on the LCSRs are given as [121]

$$V^{B\rho}(q^2) = \frac{1.045}{1-q^2/(5.32)^2}-\frac{0.721}{1-q^2/38.34},$$
$$A_0^{B\rho}(q^2) = \frac{1.527}{1-q^2/(5.28)^2}-\frac{1.220}{1-q^2/33.36},$$
$$A_1^{B\rho}(q^2) = \frac{0.220}{1-q^2/37.51},$$
$$A_2^{B\rho}(q^2) = \frac{0.009}{1-q^2/40.82}-\frac{0.212}{(1-q^2/40.82)^2}. \tag{95}$$

Recently, the $B\to D^{(*)}$ form factors associated with various types of currents, which are formulated in the heavy quark effective theory (HQET) [122], were studied up to $O(\Lambda_{QCD}/m_{b,c})$ and $O(\alpha_s)$ in Ref. [18], where several fit scenarios were shown. We summarize the relevant results of Ref. [18] with the "th:$\mathrm{L_{w\geq 1}}$ + SR" scenario in the Appendix, where the th:$\mathrm{L_{w\geq 1}}$ + SR scenario combines the QCD sum rule constraints and the QCD lattice data [16]. The parametrizations of HQET form factors are different from those shown in Eqs. (26) and (27), and

their relations can be straightforwardly found as follows: For $B \to D$, they are

$$
\begin{aligned}
f_1^{BD}(q^2) &= \frac{1}{2\sqrt{m_B m_D}}[(m_B + m_D)h_+(w) \\
&\quad - (m_B - m_D)h_-(w)], \\
f_0^{BD}(q^2) &= \frac{1}{2\sqrt{m_B m_D}}\left[\frac{(m_B + m_D)^2 - q^2}{m_B + m_D}h_+(w)\right. \\
&\quad \left. + \frac{q^2 - (m_B - m_D)^2}{m_B - m_D}h_-(w)\right],
\end{aligned} \tag{96}
$$

while for $B \to D^*$ they can be written as

$$
\begin{aligned}
V^{BD^*}(q^2) &= \frac{m_B + m_{D^*}}{2\sqrt{m_B m_{D^*}}}h_V(w), \\
A_0^{BD^*}(q^2) &= \frac{1}{2\sqrt{m_B m_{D^*}}}\left[\frac{(m_B + m_{D^*})^2 - q^2}{2m_{D^*}}h_{A_1}(w)\right. \\
&\quad - \frac{m_B^2 - m_{D^*}^2 + q^2}{2m_B}h_{A_2}(w) \\
&\quad \left. - \frac{m_B^2 - m_{D^*}^2 - q^2}{2m_{D^*}}h_{A_3}(w)\right], \\
A_1^{BD^*}(q^2) &= \frac{1}{2\sqrt{m_B m_{D^*}}}\frac{(m_B + m_{D^*})^2 - q^2}{m_B + m_{D^*}}h_{A_1}(w), \\
A_2^{BD^*}(q^2) &= \frac{m_B + m_{D^*}}{2\sqrt{m_B m_{D^*}}}\left[\frac{m_{D^*}}{m_B}h_{A_2}(w) + h_{A_3}(w)\right],
\end{aligned} \tag{97}
$$

where $w = (m_B^2 + m_{D^{(*)}}^2 - q^2)/(2m_B m_{D^{(*)}})$ and the h_i functions and their relations to the leading and subleading Isgur-Wise functions can be found in the Appendix.

B. Case with $\chi^d_{bq'} \neq 0$ and $\chi^u_{tt,ct} = \chi^d_{bb} = \chi^\ell_\ell = 0$

The free parameters involved in this study are χ^u_{tt}, $\chi^u_{ct,tc}$, $\chi^u_{ut,tu}$, χ^d_{bb}, $\chi^d_{bs,sb}$, $\chi^d_{bd,db}$, t_β, and the scalar masses $m_{H,A,H^\pm}$. To reduce the number of free parameters without the loss of generality, we adopt $\chi^q_{ij} = \chi^q_{ji}$ and take the new free parameters to be real numbers with the exception of $\chi^u_{tu,ut}$. Thus, the parameters $\chi^d_{db,sb}$ and χ^u_{tc} in leptonic $B_q^- \to \ell\bar{\nu}$ become correlated to $\chi^d_{bd,bs}$ and χ^u_{ct} in the $\Delta B = 2$ and $b \to s\gamma$ processes.

According to Eq. (78), it can be seen that the involving parameters in S-mediated $\Delta B = 2$ processes are related only to χ^d_{bs} and χ^d_{bd}. To understand how strict the experimental bounds on the $\chi^d_{bq'}$ are, we first discuss the simple situation with $\chi^u_{tt,ct} = \chi^d_{bb} = 0$. Thus, the contours of $|1 + \Delta^{S,H^\pm}_{d[s]}|$ as a function of $\chi^d_{bd[s]}$ and $\tan\beta$ are shown in Fig. 4(a) [Fig. 4(b)], where the solid and dashed lines denote the tree-level S-mediated and loop $H^\pm$-mediated effects, respectively, and $m_H = m_A = m_{H^\pm} = 600$ GeV is used. From the plots, we can see that the tree-induced ΔM_s^S gives a stronger constraint in the region of $\chi^d_{bs} > 0$. However, in the regions of $\chi^d_{bd} > 0$ and $\chi^d_{bq'} < 0$, the $H^\pm$ contributions to $B_{q'}$ mixings become dominant. In addition to the $\sqrt{x_b x_{q'}}$ suppression in $\Delta M^S_{q'}$, the loop effect can be over the tree effect, because $\chi^d_{bq'}$ in $\Delta M^{H^\pm}_{q'}$ is linear dependent, but it is quadratic in $\Delta M^S_{q'}$; as a result, when $\chi^d_{bq'}$ is of $O(10^{-2})$, the $\Delta M^{H^\pm}_{q'}$ can be larger than $\Delta M^S_{q'}$.

As mentioned earlier, the charged Higgs boson contributions to the $b \to q\ell\bar{\nu}$ processes are destructive in the type-II 2HDM. From Eq. (20), when $\chi^u_{tc} = \chi^d_{bb} = \chi^\ell_\ell = 0$, the sign change of $C^{R,\ell}_{qb}$ relies on the magnitude of χ^R_{qb}; however, the feasibility is excluded by the $\Delta M_{q'}$ constraint due to the result of $\chi^d_{bq'} \sim O(10^{-2})$. Hence, in such cases,

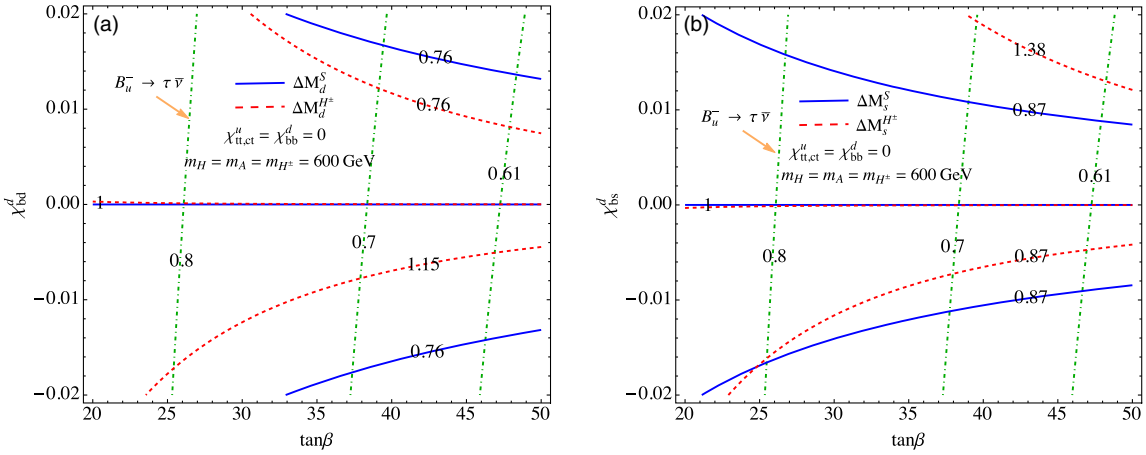

FIG. 4. Contours of $|1 + \Delta^{S,H^\pm}_{d(s)}|$ and $\mathrm{BR}(B_u^- \to \tau\bar{\nu})10^4$ as a function of $\chi^d_{bd(s)}$ and $\tan\beta$ for $\chi^u_{tt,ct} = \chi^d_{bb} = 0$, where $m_H = m_A = m_{H^\pm} = 600$ GeV is used.

the charged Higgs boson effect in the type-III model is also destructive to the SM result. To illustrate the $H^\pm$ influence on the leptonic decays, we show the contours of $\mathrm{BR}(B_u^- \to \tau\bar{\nu})$ (dot-dashed lines) in units of 10^{-4} in Figs. 4(a) and 4(b). Since χ^d_{bd} and χ^d_{bs} both appear in χ^R_{ub}, as shown in Eq. (14), when we focus on one of them, the other is set to vanish. From the plot, it can be seen that $\mathrm{BR}(B_u^- \to \tau\bar{\nu})$ is always smaller than the SM result:

$$\mathrm{BR}(B_u^- \to \tau\bar{\nu})^{\mathrm{SM}} \approx 0.89 \times 10^{-4}. \tag{98}$$

In addition, the resulting $\mathrm{BR}(B_u^- \to \tau\bar{\nu})$ is even smaller than the experimental lower bound of 1σ errors. Since similar behavior also occurs in $B_c^- \to \tau\bar{\nu}$, here, we just show the $B_u^- \to \tau\bar{\nu}$ decay. Hence, only considering the $\chi^d_{bq'}$ effect will not cause interesting implications in the leptonic B_q^- decay.

The χ^d_{bs} also affects the radiative $b \to s\gamma$ decay through the intermediates of $H^\pm$ and S shown in Figs. 2 and 3. Since the quark in the S-mediated penguin diagram is the b quark, due to the suppression of $m_b^2/m^2_{H(A)}$, the contribution of $|\chi^d_{bs}| = 0.02$ to $C^{(\prime)S}_{7\gamma}$ in Eq. (89) is of $O(10^{-4})$ and is thus negligible. According to Eq. (85), the χ^d_{bs} of the $H^\pm$ contribution appears only in $C'^{H^\pm}_{7\gamma(8G)}$ and shows up by means of $\zeta^{d*}_{ts}\zeta^d_{bb}$ and $\zeta^{d*}_{ts}\zeta^u_{tt}$. Although the former has a t_β^2 enhancement, due to the m_b^2/m_t^2 suppression in $C^{H^\pm}_{7(8),RR}$, the associated contribution is much smaller than the latter, which is insensitive to t_β. We find that, with $|\chi^d_{bs}| = 0.02$, the result is $|C'^{H^\pm}_{7\gamma}| \approx 0.012$ and is still much less than $|C^{\mathrm{SM}}_{7\gamma}|$. We note that the situation with $\chi^u_{tt,ct} = \chi^d_{bb} = 0$ is similar to the type-II model; therefore, with $|\chi^d_{bs}| < O(0.1)$, the charged Higgs boson effect on $b \to s\gamma$ is insensitive to t_β and χ^d_{bs} but is sensitive to $m_{H^\pm}$. To numerically show the result, we plot the contours of $\mathrm{BR}(\bar{B} \to X_s\gamma)$ in units of 10^{-4} in Fig. 5, where the dashed line denotes the 2σ upper limit of the experimental data and the lower bound on the charged Higgs mass is given by $m_{H^\pm} > 580$ GeV.

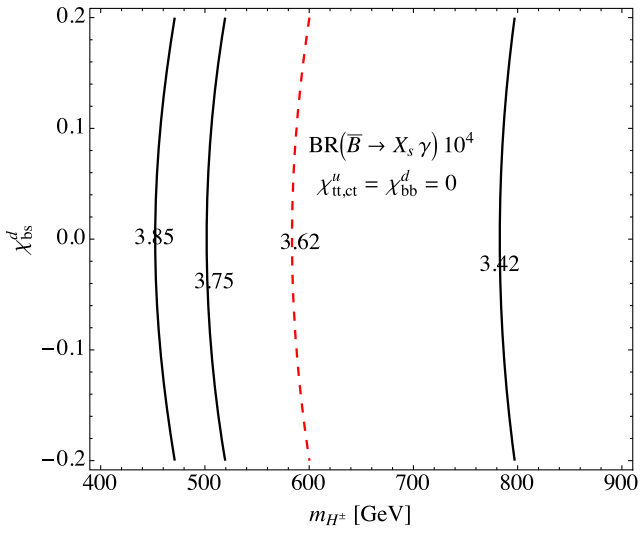

FIG. 5. Contours of $\mathrm{BR}(\bar{B} \to X_s\gamma)$ (in units of 10^{-4}) as a function of χ^d_{bs} and $m_{H^\pm}$ for $\chi^u_{tt,ct} = \chi^d_{bb} = 0$, where the dashed line denotes the 2σ upper limit of the data.

According to the above analysis, we learn that when $\chi^u_{tt,ct} = \chi^d_{bb} = 0$ is taken in the type-III 2HDM, due to the strict limits of ΔM_d and ΔM_s, the χ^d_{bd} and χ^d_{bs} effects contributing to $B_q^- \to \ell\bar{\nu}$ and $b \to s\gamma$ are small and have no interesting implications on the phenomena of interest. For simplicity, we thus take $\chi^d_{bd} = \chi^d_{bs} = 0$ in the following analysis; that is, we consider only the charged Higgs boson contributions.

C. Correlation with the constraint from the $H/A \to \tau^+\tau^-$ limits

In the 2HDM, $m_{H^\pm}$ indeed correlates with $m_{H(A)}$. According to the study in Ref. [5], the allowed mass difference can be $m_H - m_{H^\pm} \sim 100$ GeV if $m_A = m_H$ is used. Since $m_{H^\pm} = 300$ GeV is taken in our numerical analysis, the effects arisen from $m_S \equiv m_{H(A)} \sim 400$ GeV in the 2HDM cannot be arbitrarily dropped. Using this correlation, it was pointed out that the upper limit of tau-pair production through the $pp(b\bar{b}) \to H/A \to \tau^+\tau^-$ processes measured in the LHC can give a strict bound on the parameter space, which is used to explain the $R(D^{(*)})$ anomalies [123].

In order to understand how strict the constraint from the LHC data is, we now write the scalar Yukawa couplings to the quarks, proposed in Ref. [123], as

$$\mathcal{L}_{H'} \supset -Y_b\bar{Q}_3H'b_R - Y_c\bar{Q}_3\tilde{H}c_R - Y_\tau\bar{L}_3H'\tau_R + \mathrm{H.c.}, \tag{99}$$

where $H'^T = (H^+, (H+iA)/\sqrt{2})$, $Q_3^T = (V^*_{jb}u^j_L, b_L)$, and j denotes the flavor index. It can be seen that the parameters shown in the $b\bar{b} \to H/A \to \tau^+\tau^-$ processes are associated with Y_b and Y_τ. In our model, the parameters $Y_{b,\tau}$ are given, respectively, as

$$Y_b = \frac{\sqrt{2}m_b t_\beta}{v}\left(1 - \frac{\chi^d_{bb}}{s_\beta}\right),$$
$$Y_\tau = \frac{\sqrt{2}m_\tau t_\beta}{v}\left(1 - \frac{\chi^\ell_\tau}{s_\beta}\right). \tag{100}$$

Comparing with Eq. (9), it can be seen that the lepton couplings to $H(A)$ are the same as those to $H^\pm$. Because of the FCNC and CKM matrix effects, the $H^\pm c_L b_R$ coupling shown in Eq. (10) is generally different from Y_b; however, when we take $\chi^d_{bb} = \chi^d_{sb} = \chi^d_{db} = 0$, they become the same and are $Y_b = \sqrt{2}m_b t_\beta/v$.

According to the ATLAS search for the τ-pair production through the resonant scalar decays, in which the result was

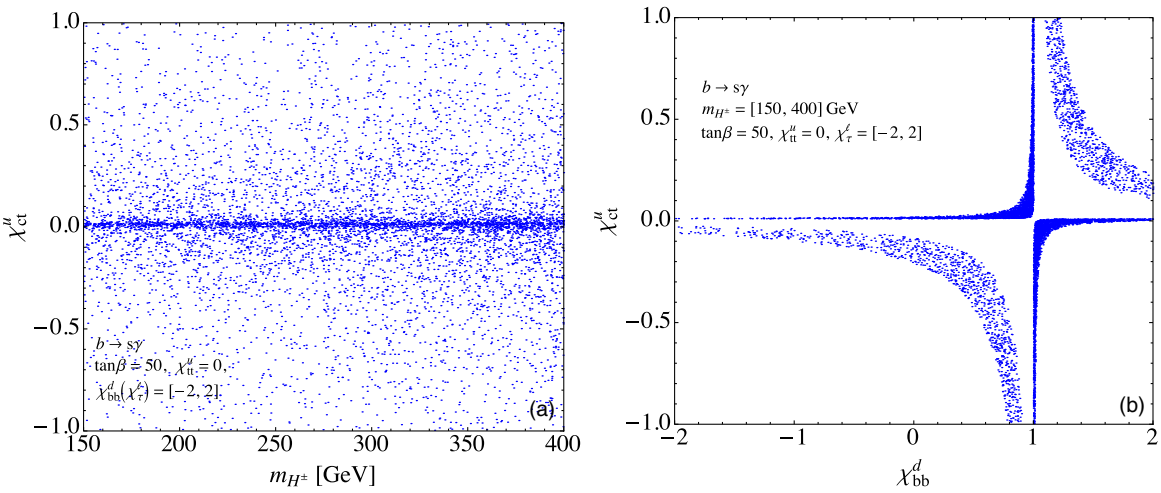

FIG. 6. Allowed parameter spaces by the $\bar{B} \to X_s\gamma$ constraint, where $\chi^u_{tt} = 0$ and $\tan\beta = 50$ are fixed.

measured at $\sqrt{s} = 13$ TeV with a luminosity of 3.2 fb^{-1}, it was shown in Ref. [123] that the allowed values of Y_b and Y_τ in Eq. (99) should satisfy $|Y_b Y_\tau| v^2/m_S^2 < 0.3$ for $m_S = 400$ GeV. Thus, using $t_\beta = 50$, we can obtain the limit from Eq. (100) as

$$|(1 - \chi^\ell_\tau/s_\beta)(1 - \chi^d_{bb}/s_\beta)| < 1.70, \qquad (101)$$

where $m_b(m_S) = 3.18$ GeV and $m_\tau = 1.78$ GeV are applied. Hence, we will take Eq. (101) as an input to bound the χ^ℓ_τ and χ^d_{bb} parameters.

D. Constraints of $b \to s\gamma$ and $B_{q'}$ mixings

From Eq. (85), there are two terms contributing to $C^{H^\pm}_{7\gamma(8G)}$, where the associated charged Higgs boson effects are $\zeta^{u*}_{ts}\zeta^u_{tt}$ and $\zeta^{u*}_{ts}\zeta^d_{bb}$. Using the definitions in Eq. (63), it can be seen that the new factor $\chi^{L*}_{ts}\chi^{u*}_{tt}/s^2_\beta$ in the first term is insensitive to $t_\beta > 10$; however, $\zeta^{u*}_{ts}\zeta^d_{bb} \propto 1 - t_\beta(\chi^{L*}_{ts}/s_\beta)(1 - \chi^d_{bb}/s_\beta)$ (unity denotes the result of the type-II model) formed in the second term can be largely changed by a large t_β. In addition, we see that $C^{H^\pm}_{7(8),LL}$ and $C^{H^\pm}_{7(8),RL}$ are negative values, and the magnitude of the former is approximately one order smaller than that of the latter; that is, $\zeta^{u*}_{ts}\zeta^d_{bb}$ indeed dominates. Because of the negative loop integral value, it can be understood that the Wilson coefficient $C^{H^\pm}_{7\gamma}(\mu_b)$ in the type-II model is the same sign as $C^{\rm SM}_{7\gamma}(\mu_b)$; thus, $m_{H^\pm}$ is severely limited, and the low bound is $m_{H^\pm} > 580$ GeV, as shown in Ref. [75] and confirmed in Fig. 5.

Because of new Yukawa couplings involved in the type-III model, e.g., $\chi^u_{tt,ct}$ and χ^d_{bb}, the $b \to s\gamma$ constraint on $m_{H^\pm}$ can be relaxed. To see the $b \to s\gamma$ constraint, we scan the parameters with the sampling points of 5×10^5, for which the results are shown in Figs. 6(a) and 6(b), where in both plots $t_\beta = 50$ is fixed, and the scanned regions of parameters are set as $m_{H^\pm} = [150,400]$ GeV, $\chi^u_{ct} = [-1, 1]$, $\chi^d_{bb} = [-2, 2]$, and $\chi^\ell_\tau = [-2, 2]$. Since χ^u_{tt} and χ^u_{ct} in χ^L_{ts} appear in addition form, we take $\chi^u_{tt} = 0$ for simplicity, although it is not necessary. From the results, it can be clearly seen that, due to the new charged Higgs boson effects, the bound on $m_{H^\pm}$ is much looser than that in the type-II model. From Fig. 6(b), the sampling points are condensed at $\chi^d_{bb} \approx 1$, because $(1 - \chi^d_{bb}/s_\beta)$ becomes small when χ^d_{bb} approaches one.

We now know that $H^\pm$ can be as light as a few hundred GeV in the type-III model. In order to include the contributions of all $\chi^d_{tt,ct}$ and χ^d_{bb} with large t_β and combine the constraints from the $\Delta B = 2$ processes shown in Eq. (76) altogether, we fix $t_\beta = 50$ and $m_{H^\pm} = 300$ GeV and use the sampling points of 5×10^5 to scan the involved parameters. The allowed parameter spaces, which consider only the $\bar{B} \to X_s\gamma$ constraint, are shown in Fig. 7(a), and those of combining the $\bar{B} \to X_s\gamma$ and $\Delta M_{d,s}$ constraints are given in Fig. 7(b), where $|\chi^u_{tt,ct}| \le 1$, $|\chi^d_{bb}| \le 1$, and $|\chi^\ell_\tau| \le 2$ have been used. Comparing Figs. 7(a) and 7(b), it can be obviously seen that $\Delta B = 2$ processes can further exclude some free parameter spaces.

E. Charged Higgs boson on the leptonic $B^-_q \to \ell\bar{\nu}$ decays

After analyzing the $b \to s\gamma$ and $\Delta B = 2$ constraints, we study the charged Higgs boson contributions to the leptonic and semileptonic B decays in the remaining part of the paper. In order to focus on the $\chi^u_{tc,tu}$ and χ^ℓ_ℓ effects, we fix $\chi^d_{bb} = \chi^d_{db,sb} = 0$, $t_\beta = 50$, and $m_{H^\pm} = 300$ in the following numerical analyses, unless stated otherwise. With the

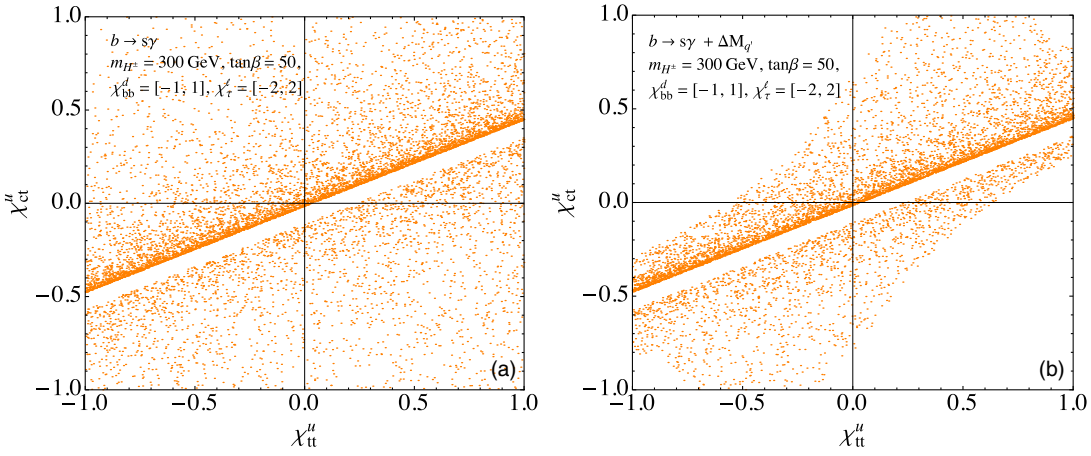

FIG. 7. Allowed parameter spaces by the constraint from (a) $\bar{B} \to X_s\gamma$ and (b) $\bar{B} \to X_s\gamma + \Delta M_{q'}$, where $\chi^d_{bb} = [-1, 1]$ and $\chi^\ell_\tau = [-2, 2]$ are taken and $\tan\beta = 50$ and $m_{H^\pm} = 300$ GeV are used.

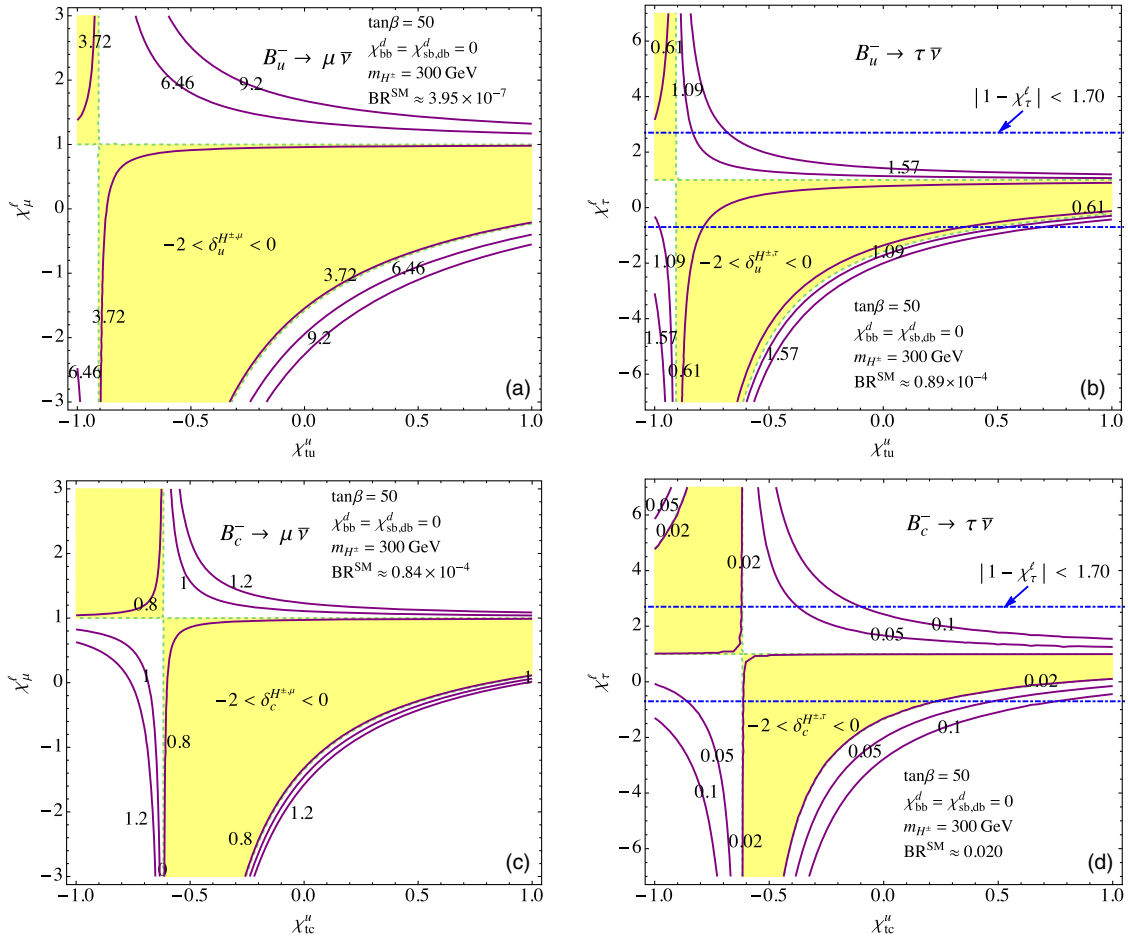

FIG. 8. Contours for (a) $\mathrm{BR}(B_u^- \to \mu\bar{\nu})$ in units of 10^{-7}, (b) $\mathrm{BR}(B_u^- \to \tau\bar{\nu})$ in units of 10^{-4}, (c) $\mathrm{BR}(B_c^- \to \mu\bar{\nu})$ in units of 10^{-4}, and (d) $\mathrm{BR}(B_c^- \to \tau\bar{\nu})$, where the hatched region denotes $-2 < \delta_q^{H^\pm,\ell} < 0$. The dot-dashed lines in (b) and (d) are the constraint from Eq. (101).

TABLE II. Branching ratio for $\bar{B}_d \to (\pi^+, \rho^+)\ell\bar{\nu}$ based on the LCSR form factors and the measured data.

Model	$\bar{B}_d \to \pi^+ e(\mu)\bar{\nu}$	$\bar{B}_d \to \pi^+\tau\bar{\nu}$	$\bar{B}_d \to \rho^+ e(\mu)\bar{\nu}$	$\bar{B}_d \to \rho^+\tau\bar{\nu}$
SM	1.43×10^{-4}	1.05×10^{-4}	2.87×10^{-4}	1.68×10^{-4}
Exp [70]	$(1.45 \pm 0.05) \times 10^{-4}$	$<2.5 \times 10^{-4}$	$(2.94 \pm 0.21) \times 10^{-4}$	None

numerical inputs, the BRs of leptonic $B^-_{u,c}$ decays in the SM are estimated as

$$\begin{aligned}
&\mathrm{BR}(B_u^- \to \mu\bar{\nu})^{\mathrm{SM}} \approx 3.95 \times 10^{-7},\\
&\mathrm{BR}(B_u^- \to \tau\bar{\nu})^{\mathrm{SM}} \approx 0.98 \times 10^{-4},\\
&\mathrm{BR}(B_c^- \to \mu\bar{\nu})^{\mathrm{SM}} \approx 0.84 \times 10^{-4},\\
&\mathrm{BR}(B_c^- \to \tau\bar{\nu})^{\mathrm{SM}} \approx 0.02.
\end{aligned} \tag{102}$$

From Eqs. (23) and (25), there are two ways to enhance the BR of $B_q^- \to \ell\bar{\nu}$: One is $\delta_q^{H^\pm,\ell} > 0$, and the other is $\delta_q^{H^\pm,\ell} < -2$. For clarity, the contours for $B_u^- \to (\mu,\tau)\bar{\nu}$ and $B_c^- \to (\mu,\tau)\bar{\nu}$ as a function of $\chi^\ell_{\mu,\tau}$ and $\chi^u_{tu,tc}$ are shown in Figs. 8(a)–8(d), where we have chosen the weak phase of χ^{u*}_{tu} to be the same as V_{ub} so that $\delta_u^{H^\pm,\ell}$ is real, where the hatched regions denote $-2 < \delta_q^{H^\pm,\ell} < 0$ and the dot-dashed lines are the constraint from the $H/A \to \tau^+\tau^-$ decays, shown in Eq. (101). $\delta_q^{H^\pm,\ell} > 0$ occurs in the up-right and down-left unhatched regions, while other unhatched regions are for $\delta_q^{H^\pm,\ell} < -2$. From the results, if we do not further require the values of $\delta_q^{H^\pm,\ell}$, both $\delta_q^{H^\pm,\ell} > 0$ and $\delta_q^{H^\pm,\ell} < -2$ can significantly enhance the $\mathrm{BR}(B_q^- \to \ell\bar{\nu})$. From Figs. 8(b) and 8(d), although the measured values of $\mathrm{BR}(B_u^- \to \tau\bar{\nu})$ and the indirect upper bound of $\mathrm{BR}(B_c^- \to \tau\bar{\nu}) < 10\%$ [65] can constrain the parameters to be a small region, the constraint from the $pp \to H/A \to \tau^+\tau^-$ processes further excludes the region of $\chi^\ell_\tau < -0.7$. If $\mathrm{BR}(B_u^- \to \mu\bar{\nu})$ can be measured at Belle II, the χ^ℓ_μ parameter can be further constrained.

F. Charged Higgs boson on the $\bar{B}_d \to (\pi^+, \rho^+)\ell\bar{\nu}$ decays

Compared to the charged B-meson decays, $\bar{B}_d \to (\pi^+, \rho^+)\ell\bar{\nu}$ have larger BRs; thus, we discuss the neutral B-meson decays. With the LCSR form factors, the BRs of these decays in the SM are given in Table II, where the current measurements of light lepton channels are also shown. From the table, we can see that the BRs for $\bar{B}_d \to (\pi^+, \rho^+)\ell\bar{\nu}$ (here $\ell = e, \mu$) in the SM are close to the observed values. Because of the $H^\pm$ Yukawa coupling to the lepton being proportional to $t_\beta m_\ell/v$, the charged Higgs boson contributions to the light lepton channels are small. Thus, we can conclude that the consistency between the data and the SM verifies the reliability of the LCSR form factors in the $\bar{B} \to (\pi, \rho)$ transitions. In the following analysis, we study the charged Higgs boson influence on the τ-lepton modes and their associated observables.

From Table II, the ratios of branching fractions for $\bar{B}_d \to (\pi^+, \rho^+)\ell\bar{\nu}$ in the SM can be estimated as

$$\begin{aligned}
R(\pi) &= \frac{\mathrm{BR}(\bar{B}_d \to \pi^+\tau\bar{\nu})}{\mathrm{BR}(\bar{B}_d \to \pi^+ e(\mu)\bar{\nu})} \approx 0.731,\\
R(\rho) &= \frac{\mathrm{BR}(\bar{B}_d \to \rho^+\tau\bar{\nu})}{\mathrm{BR}(\bar{B}_d \to \rho^+ e(\mu)\bar{\nu})} \approx 0.585.
\end{aligned} \tag{103}$$

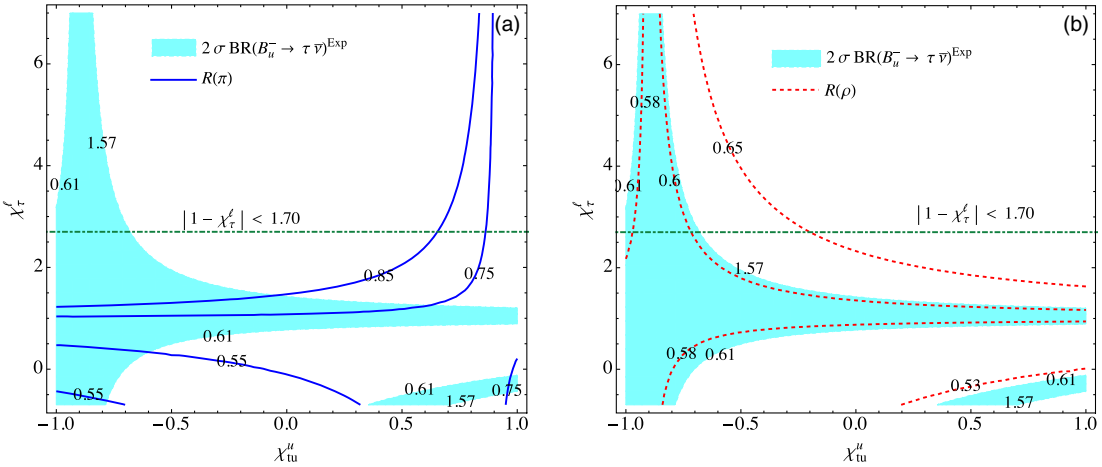

FIG. 9. Contours for (a) $R(\pi)$ and (b) $R(\rho)$ as a function of χ^u_{tu} and χ^ℓ_τ, where the hatched regions are the observed $B_u^- \to \tau\bar{\nu}$ within 2σ errors and the dot-dashed lines denote the constraint from the $pp \to H/A \to \tau^+\tau^-$ processes.

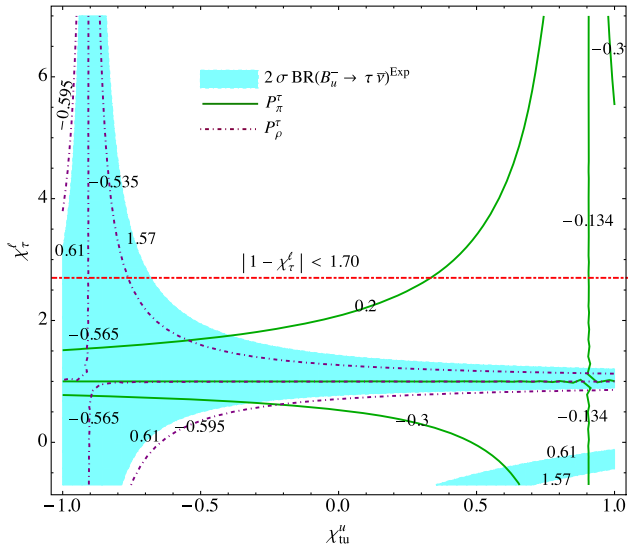

FIG. 10. Contours for P_π^τ and P_ρ^τ.

Using Eq. (51), the contours for $R(\pi)$ and $R(\rho)$ as a function of χ_{tu}^u and χ_τ^ℓ are shown in Figs. 9(a) and 9(b), respectively, where the hatched regions denote BR$(B_u^- \to \tau\bar{\nu})^{\rm exp}$ with 2σ errors. According to the results, it can be found that, due to the constraint of $B_u^- \to \tau\bar{\nu}$, the allowed $R(\rho)$ is limited to being a very narrow range of $\sim(0.58, 0.60)$. From Fig. 9(b), since $R(\rho)$ and BR$(B_u^- \to \tau\bar{\nu})$ do not overlap at the down-right region, basically, this $\delta_u^{H^\pm,\tau} < 0$ region has been excluded by the data of $B_u^- \to \tau\bar{\nu}$. The reason why $B_u^- \to \tau\bar{\nu}$ gives a strict limit on $\bar{B}_d \to \rho^+\tau\bar{\nu}$ can be understood from Eq. (30), where both decays share the same $C_{ub}^{R,\tau} - C_{ub}^{L,\tau}$ charged Higgs boson effect. On the contrary, $\bar{B}_d \to \pi^+\tau\bar{\nu}$ is related to $C_{ub}^{R,\tau} + C_{ub}^{L,\tau}$, so $R(\pi)$ can have a wider range of values. Although the $pp \to H/A \to \tau^+\tau^-$ constraint (dot-dashed line) does not affect the allowed values of $R(\pi)$ and $R(\rho)$, it can reduce the allowed region of χ_τ^ℓ.

Although it is difficult to measure the lepton polarization in the $\bar{B}_d \to (\pi^+, \rho^+)\ell\bar{\nu}$, we theoretically investigate the charged Higgs boson contributions to the semileptonic B decays. Using Eqs. (58) and (59), the lepton helicity asymmetries in the SM can be found as

$$P_\pi^{e(\mu)} \approx -1(-0.986), \qquad P_\pi^\tau \approx -0.134,$$
$$P_\rho^{e(\mu)} \approx -1(-0.992), \qquad P_\rho^\tau \approx -0.565. \tag{104}$$

Because of the fact that the helicity asymmetry is strongly dependent on m_ℓ, it can be understood that only $\tau\bar{\nu}$ modes can be away from unity. All lepton polarizations show negative values, because the $V-A$ current in the SM dominates. The sign of τ-lepton polarization in $\bar{B} \to D\tau\bar{\nu}$ can be flipped to be a positive sign. In order to show the $H^\pm$ influence, the contours for P_π^τ and P_ρ^τ as a function of χ_{tu}^u and χ_τ^ℓ are given in Fig. 10, where the constraint from $pp \to H/A \to \tau^+\tau^-$ (dot-dashed line) with $\chi_{bb}^d = 0$ is also shown. With the $B_u^- \to \tau\bar{\nu}$ constraint, the allowed values of P_ρ^τ are limited in a narrow region around the SM value. However, the allowed values of P_π^τ are wider and can have both negative and positive signs.

The lepton FBAs are also interesting observables in the semileptonic B decays. Following the formulas in Eq. (61), we show the FBAs of $\bar{B}_d \to \pi^+\tau\bar{\nu}$ and $\bar{B}_d \to \rho^+\tau\bar{\nu}$ as a function of q^2 in Figs. 11(a) and 11(b), respectively, where the solid line is the SM and the dashed line is the type-II model. For the type-III 2HDM, we select two benchmarks

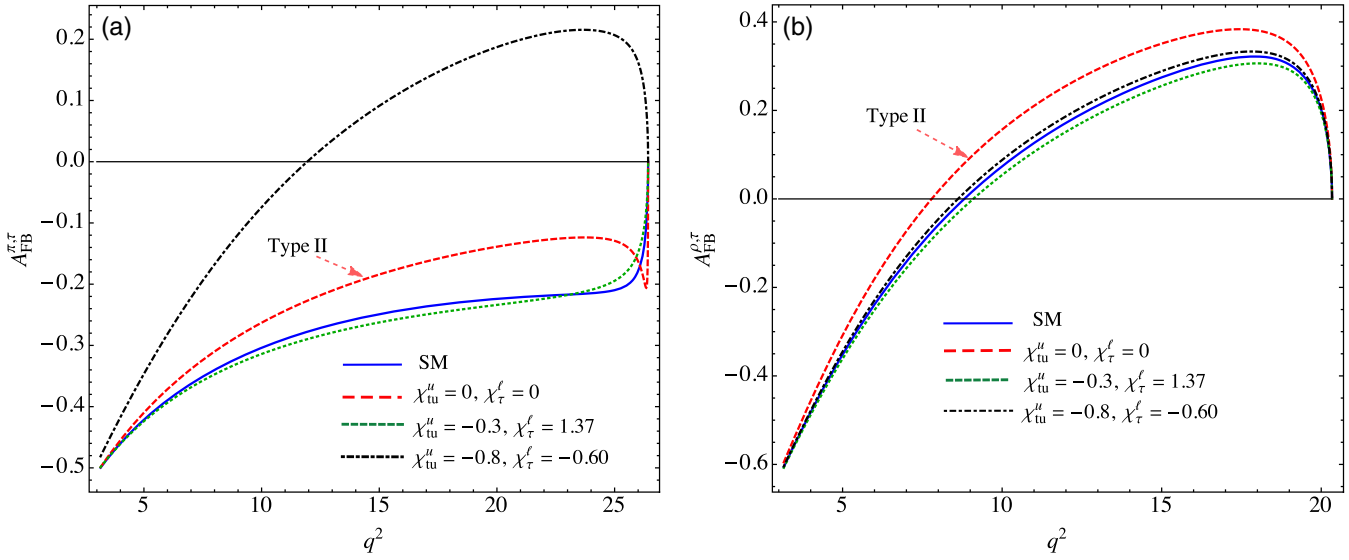

FIG. 11. q^2-dependent lepton forward-backward asymmetry for (a) $\bar{B}_d \to \pi^+\tau\bar{\nu}$ and (b) $\bar{B}_d \to \rho^+\tau\bar{\nu}$ in the SM (solid line), type-II (dashed line), and type-III 2HDM (dotted and dot-dashed lines).

TABLE III. Branching ratios for $B_u^- \to (D^0, D^{*0})\ell\bar{\nu}$ in the SM and the associated experimental data.

Model	$B_u^- \to D^0\ell\bar{\nu}$	$B_u^- \to D^0\tau\bar{\nu}$	$B_u^- \to D^{*0}\ell\bar{\nu}$	$B_u^- \to D^{*0}\tau\bar{\nu}$
SM	2.10%	6.48×10^{-3}	5.74%	1.48%
Exp [70]	$(2.27 \pm 0.11)\%$	$(7.7 \pm 2.5) \times 10^{-3}$	$(5.69 \pm 0.19)\%$	$(1.88 \pm 0.20)\%$

that obey the $B_u^- \to \tau\bar{\nu}$ constraint as follows: The dotted line is $\chi_{tu}^u = -0.3$ and $\chi_\tau^\ell = 1.37$, which lead to $R(\pi) \approx 0.855$ and $R(\rho) \approx 0.595$; and the dot-dashed line denotes $\chi_{tu}^u = -0.8$ and $\chi_\tau^\ell = -0.60$, which lead to $R(\pi) \approx 0.550$ and $R(\rho) \approx 0.577$. From Fig. 11(a), we can see that $A_{FB}^{\pi,\tau}$ can be largely changed by the charged Higgs boson effect; in other words, a zero point can occur in $A_{FB}^{\pi,\tau}$, where the zero point usually occurs in the ρ^+ channel, as shown in Fig. 11(b). Hence, we can use the characteristics of FBA to test the SM by examining the shape of $A_{FB}^{\pi,\tau}$. From Fig. 11(b), due to the strict limit of $B_u^- \to \tau\bar{\nu}$, the shape change of $A_{FB}^{\rho,\tau}$ in the type-III model is small.

G. Charged Higgs boson on the $B_u^- \to (D^0, D^{*0})\ell\bar{\nu}$ decays

From Eq. (51) and the HQET form factors introduced previously, the BRs for the $B_u^- \to (D^0, D^{*0})\ell\bar{\nu}$ decays in the SM can be estimated, as shown in Table III, where the current experimental results are also included [70]. It can be seen that the BRs of the light lepton channels in the SM are consistent with the experimental data; however, the $\tau\bar{\nu}$ mode results are somewhat smaller than those in the current data. The ratios of branching fractions are obtained as $R(D)^{\rm SM} \approx 0.309$ and $R(D^*)^{\rm SM} \approx 0.257$, which are consistent with the results obtained in the literature.

As discussed before, the $H^\pm$ contributions to $B_u^- \to D^0\ell\bar{\nu}$ and $B_u^- \to D^{*0}\ell\bar{\nu}$ are associated with $C_{cb}^{R,\ell} + C_{cb}^{L,\ell}$ and $C_{cb}^{R,\ell} - C_{cb}^{L,\ell}$, respectively, and the same factor $C_{cb}^{R,\ell} - C_{cb}^{L,\ell}$ also appears in the $B_c^- \to \ell\bar{\nu}$ decay; that is, $R(D^*)$ and $\mathrm{BR}(B_c^- \to \tau\bar{\nu})$ have a strong correlation [42,50,65]. Although there is no direct measurement of the $B_c^- \to \tau\bar{\nu}$ decay, the indirect upper limit on the $\mathrm{BR}(B_c^- \to \tau\bar{\nu})$ can be obtained by the lifetime of B_c with a result of 30% [50] and the LEP1 data [65] with a result of 10%. We show $R(D)$ and $R(D^*)$ as a function of χ_{tc}^u and χ_τ^ℓ in Fig. 12 (left panel), where the shaded regions denote the results for $0.1 \le \mathrm{BR}(B_c^- \to \tau\bar{\nu}) \le 1$ and the dot-dashed line is the upper bound from the $pp \to H/A \to \tau^+\tau^-$ processes with $\chi_{bb}^d = 0$. For clarity, we also show the regions for $\delta_c^{H^\pm} > 0$ and $\delta_c^{H^\pm} < -2$ in the plot. From the results, we can clearly see that, due to the limit of $\mathrm{BR}(B_c^- \to \tau\bar{\nu}) < 10\%$, the maximal value of the charged Higgs boson contribution to $R(D^*)$ can be only approximately 0.265; however, the values of $R(D)$ can be within a 1σ world average.

According to Eqs. (58) and (59), it is expected that the helicity asymmetry of a light lepton will negatively approach unity and that only τ-lepton polarizations can significantly deviate from one. With HQET form factors, the lepton polarizations in the SM are estimated as

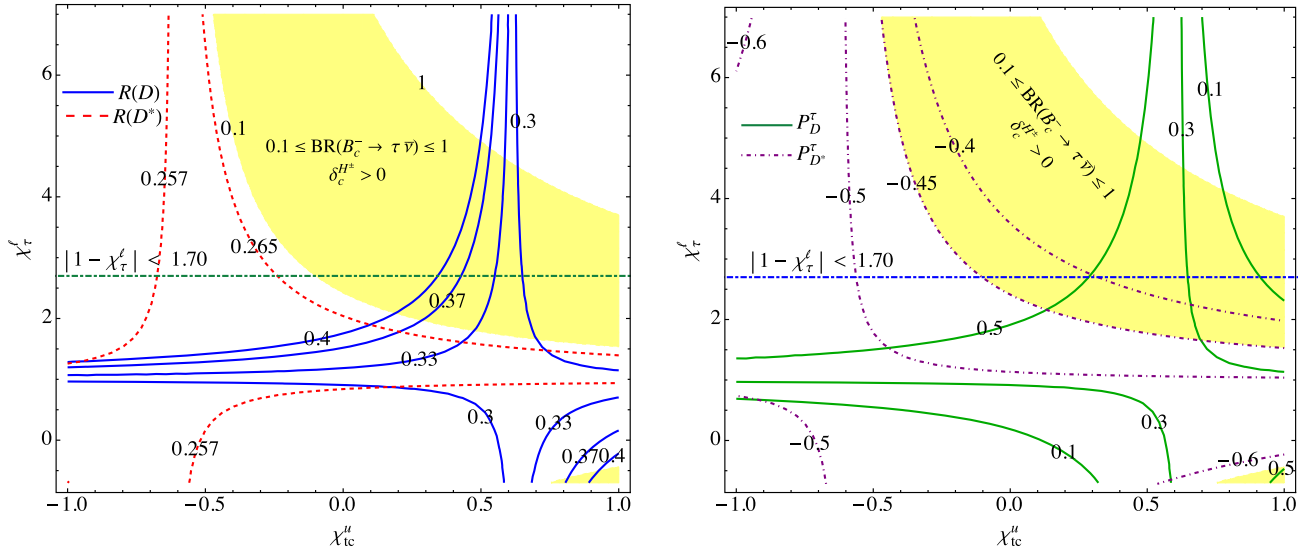

FIG. 12. Left panel: $R(D)$, $R(D^*)$, and $\mathrm{BR}(B_c^- \to \tau\bar{\nu})$ as a function of χ_{tc}^u and χ_τ^ℓ, where the shaded regions denote the situation of $0.1 \le \mathrm{BR}(B_c^- \to \tau\bar{\nu}) \le 1$. Right panel: Contours for P_D^τ and $P_{D^*}^\tau$. The dot-dashed lines are the constraint shown in Eq. (101) with $\chi_{bb}^d = 0$.

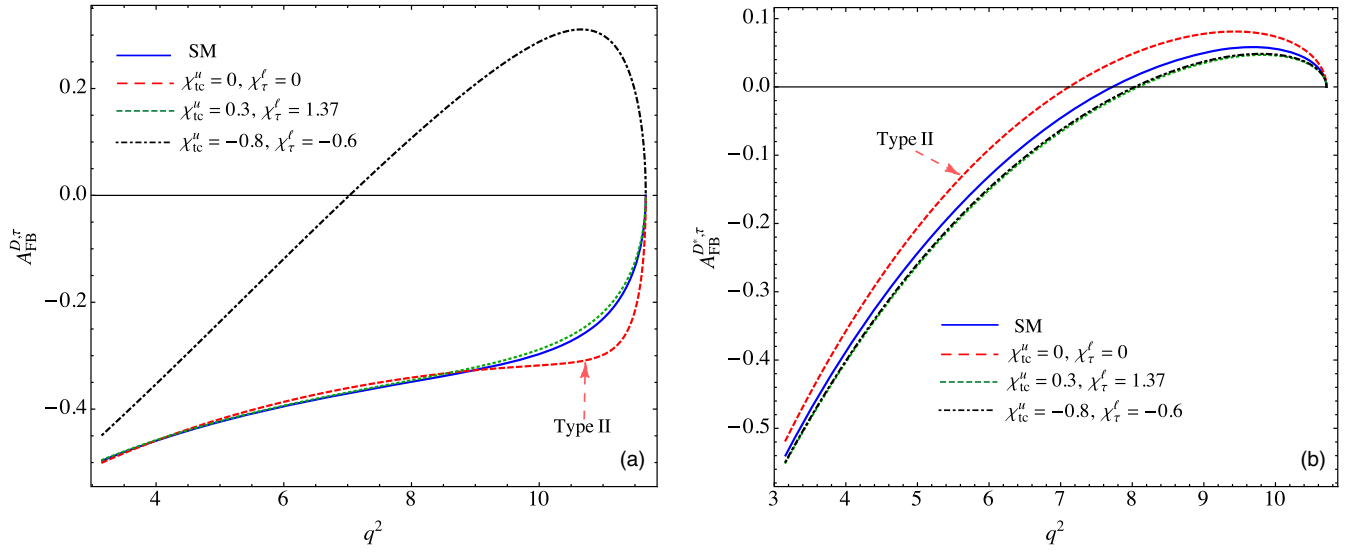

FIG. 13. τ-lepton forward-backward asymmetry as a q^2 dependence for (a) $B_u^- \to D^0\tau\bar{\nu}$ and (b) $B_u^- \to D^{*0}\tau\bar{\nu}$, where the solid line is from the SM; the dashed line is the type-II model with $R(D^{(*)}) \approx 0.220(0.252)$; the dotted (dot-dashed) line is from $\chi^u_{tc} = 0.3$ (-0.8) and $\chi^\ell_\tau = 1.37$ (-0.60), and the corresponding results are $R(D) \approx 0.331$ (0.145) and $R(D^*) \approx 0.262$ (0.261).

$$P_D^{e(\mu)} \approx -1(-0.962), \qquad P_D^\tau \approx 0.320,$$
$$P_{D^*}^{e(\mu)} \approx -1(-0.986), \qquad P_{D^*}^\tau \approx -0.506, \quad (105)$$

where Belle's current measurement is $P_{D^*}^\tau = -0.38 \pm 0.51^{+0.21}_{-0.16}$ [12]. Intriguingly, the sign of P_D^τ is opposite to that of $P_{D^*}^\tau$, and the situation is different from the negative sign in P_π^τ. We find that the origin of the difference in sign between P_π^τ and P_D^τ is from the meson mass. Because of $m_D \gg m_\pi$, the positive helicity becomes dominant in $B_u^- \to D^0\tau\bar{\nu}$. To see the influence of the charged Higgs boson on the τ polarizations, we show the contours for P_D^τ and $P_{D^*}^\tau$ in the right panel in Fig. 12. With the limit of $\mathrm{BR}(B_c^- \to \tau\bar{\nu}) < 10\%$, it is found that P_D^τ can be largely changed by the charged Higgs boson effect, and the allowed range of $P_{D^*}^\tau$ is narrow and can be changed by $\sim$10%, where the change in $R(D^*)$ from the same $H^\pm$ effects is only $\sim$3%.

Finally, we discuss the lepton FBAs in the $B_u^- \to (D^0, D^{*0})\ell\bar{\nu}$ decays. As discussed in the $\bar{B}_d \to (\pi^+, \rho^+)\ell\bar{\nu}$ decays, only $A_{FB}^{D^{(*)},\tau}$ are sensitive to the charged Higgs boson effects. Thus, we show the $A_{FB}^{D^{[*]},\tau}$ as a function of q^2 in Fig. 13(a) [Fig. 13(b)], where the solid line denotes the SM result and the dashed line is the type-II model with $R(D^{(*)}) = 0.220$ (0.252). We use two benchmarks to show the effects of the type-III 2HDM: The dotted line is the result of $\chi^u_{tc} = 0.3$ and $\chi^\ell_\tau = 1.37$ which cause $R(D^{(*)}) \approx 0.331(0.262)$, and the dot-dashed line denotes $\chi^u_{tc} = -0.8$ and $\chi^\ell_\tau = -0.60$ which cause $R(D^{(*)}) \approx 0.145(0.261)$. From Fig. 13(a), similar to the case in $A_{FB}^{\pi,\tau}$, $A_{FB}^{D,\tau}$ can have a vanishing point in the type-III model when it crosses the q^2 axis. Usually, the zero point occurs in $B_u^- \to D^{*0}\ell\bar{\nu}$, and the position of the zero point is sensitive to the new physics, as shown in Fig. 13(b). Hence, based on our analysis, we can use this characteristics of FBA to test the SM.

VI. CONCLUSION

We studied the constraints of the $b \to s\gamma$ and $\Delta B = 2$ processes in the type-III 2HDM with the Cheng-Sher ansatz, where the detailed analyses included the neutral scalars H and A (tree + loop) and charged Higgs boson (loop) effects. It was found that the tree-induced $\Delta B = 2$ processes produce strong constraints on the parameters χ^d_{db} and χ^d_{sb}, and, due to the $m_b/m_{H(A)}$ suppression, the loop-induced $b \to s\gamma$ process by the same H, A effects is small. When we ignore the $\chi^d_{db,sb}$ effects, the dominant contributions to the rare processes are the charged Higgs boson.

We demonstrated that due to the new parameters involved, i.e., $\chi^u_{tt,tc}$ and χ^d_{bb}, the mass of the charged Higgs boson in the type-III model can be much lighter than that in the type-II model when the $b \to s\gamma$ constraint is satisfied. Taking $m_{H^\pm} = 300$ GeV and $\tan\beta = 50$, we comprehensively studied the charged Higgs boson contributions to the leptonic $B_{u,c}^- \to \ell\bar{\nu}$ and semileptonic $\bar{B}_{u,d} \to (P, V)\ell\bar{\nu}$ $(P = \pi^+, D^0; V = \rho^+, D^{*0})$ decays in the generic 2HDM.

In addition to the constraints from the low-energy flavor physics, such as $B_{d,s}$-$\bar{B}_{d,s}$ mixings and $B_s \to X_s\gamma$, we also consider the constraint from the upper limit of $pp \to H/A \to \tau^+\tau^-$ measured in the LHC. It was found that the tau-pair production cross section can further constrain the χ^ℓ_τ parameter to be $|1 - \chi^\ell_\tau| < 1.70$ with $\chi^d_{bb} = 0$.

The main difference in the $b \to (u, c)\ell\bar{\nu}$ decays between type II and type III is that the former is always destructive to

the SM results and the latter can make the situation constructive. Therefore, $\mathrm{BR}(B_u^- \to (\mu,\tau)\bar{\nu})$ can be enhanced from the SM results to the current experimental observations. Although $B_c^- \to \tau\bar{\nu}$ has not yet been observed, the charged Higgs boson can also enhance its branching ratio from 2% to the upper limit of 10%, where the upper limit is obtained from the LEP1 data.

Since a heavy lepton can be significantly affected by the charged Higgs boson, we analyzed the potential observables in the $\bar{B}_d \to (\pi^+,\rho^+)\tau\bar{\nu}$ and $B_u^- \to (D^0, D^{*0})\tau\bar{\nu}$ decays. It was shown that, since $B_{u(c)}^- \to \tau\bar{\nu}$ and $B_u^- \to \rho^+(D^{*0})\tau\bar{\nu}$ are strongly correlated to the same charged Higgs boson effects, the allowed $R(\rho^+)$, $R(D^*)$, P_ρ^τ, $P_{D^*}^\tau$, and $A_{FB}^{\rho,\tau}$ are very limited in terms of deviating from the SM. Although the change in $A_{FB}^{D^*,\tau}$ is not large, the deviation is still sizable. In contrast, the observables in the π^+ and D^0 channels are sensitive to the charged Higgs boson effects and exhibit significant changes.

ACKNOWLEDGMENTS

This work was partially supported by the Ministry of Science and Technology of Taiwan, under Grant No. MOST-106-2112-M-006-010-MY2 (C.-H. C.).

APPENDIX: VERTICES AND FORM FACTORS

1. $H^\pm$ Yukawa couplings to the quarks

According to Eq. (6), we write the charged Higgs Yukawa couplings to the quarks as

$$\begin{aligned}
\mathcal{L}_{Y,q}^{H^\pm} &= \frac{\sqrt{2}}{v}\bar{u}_{iR}C_{u_i d_k}^L d_{kL}H^+ + \frac{\sqrt{2}}{v}\bar{u}_{iL}C_{u_i d_k}^R d_{kR}H^+ + \text{H.c.},\\
C_{u_i d_k}^L &= \left(\frac{m_{u_i}}{t_\beta}\delta_{ij} - \frac{\sqrt{m_{u_i}m_{u_j}}}{s_\beta}\chi_{ji}^{u*}\right)V_{u_j d_k},\\
C_{u_i d_k}^R &= V_{u_i d_j}\left(t_\beta m_{d_j}\delta_{jk} - \frac{\sqrt{m_{d_j}m_{d_k}}}{c_\beta}\chi_{jk}^{d}\right),
\end{aligned} \tag{A1}$$

where u_j and d_j denote the sum of all possible up- and down-type quarks, respectively. We showed the b-quark-related Yukawa couplings in the text. Here, we discuss the $H^\pm$ Yukawa couplings to d and s quarks. In the numerical discussions, we used $m_{u(d)} \approx 5.4$ MeV, $m_s \approx 0.1$ GeV, $m_c \approx 1.3$ GeV, and $m_t \approx 165$ GeV.

a. udH^+ vertex

Following Eq. (A1), we write the C_{ud}^L coupling as

$$\begin{aligned}
\frac{\sqrt{2}}{v}C_{ud}^L = \frac{\sqrt{2}}{v}\Bigg[&\left(\frac{1}{t_\beta} - \frac{\chi_{uu}^{u*}}{s_\beta}\right)m_u V_{ud} - \frac{\sqrt{m_u m_c}}{s_\beta}\chi_{cu}^{u*}V_{cd}\\
&- \frac{\sqrt{m_u m_t}}{s_\beta}\chi_{tu}^{u*}V_{td}\Bigg].
\end{aligned} \tag{A2}$$

It can be seen that the first and third terms are negligible due to the suppressions of m_u/v and $\sqrt{m_u/m_t}V_{td}$, respectively. Although the second term is somewhat larger, it is also negligible based on the result of $\sqrt{2m_u m_c}V_{cd}/v \sim -1.0\times10^{-4}$. Hence, it is a good approximation to take $C_{ud}^L \sim 0$. For the C_{ud}^R coupling, it can be decomposed to be

$$\begin{aligned}
\frac{\sqrt{2}}{v}C_{ud}^R &= \frac{\sqrt{2}}{v}\Bigg[t_\beta m_d V_{ud}\left(1 - \frac{\chi_{dd}^d}{s_\beta}\right) - \frac{\sqrt{m_s m_d}}{c_\beta}\chi_{sd}^d V_{us}\\
&\quad - \frac{\sqrt{m_b m_d}}{c_\beta}\chi_{bd}^d V_{ub}\Bigg]\\
&\approx \sqrt{2}\frac{m_d t_\beta}{v}V_{ud}\left(1 - \frac{\chi_{ud}^R}{s_\beta}\right),\\
\chi_{ud}^R &= \chi_{dd}^d + \sqrt{\frac{m_s}{m_d}}\frac{V_{us}}{V_{ud}}\chi_{ds}^d,
\end{aligned} \tag{A3}$$

where we have neglected the V_{td} contribution in χ_{ud}^R. Taking $t_\beta \sim 50$ and $|1 - \chi_{ud}^R/s_\beta| \sim 2$, we obtain $C_{ud}^R \sim 5.7\times10^{-3}$, and this charged Higgs coupling indeed is 2 orders of magnitude smaller than the charged W-gauge boson coupling of $g/\sqrt{2} \approx 0.467$. Thus, we can also take $C_{ud}^R \sim 0$ as a leading-order approximation.

b. cdH^+ vertex

From the definition in Eq. (A1), we write C_{cd}^L as

$$\begin{aligned}
\frac{\sqrt{2}}{v}C_{cd}^L = \frac{\sqrt{2}}{v}\Bigg[&\left(\frac{1}{t_\beta} - \frac{\chi_{cc}^{u*}}{s_\beta}\right)m_c V_{cd} - \frac{\sqrt{m_c m_u}}{s_\beta}\chi_{uc}^{u*}V_{ud}\\
&- \frac{\sqrt{m_c m_t}}{s_\beta}\chi_{tc}^{u*}V_{td}\Bigg]\\
&\approx -\sqrt{2}\frac{m_c}{v s_\beta}V_{cd}\chi_{cd}^L,\\
\chi_{cd}^L &= \chi_{cc}^{u*} + \sqrt{\frac{m_u}{m_c}}\frac{V_{ud}}{V_{cd}}\chi_{uc}^{u*} + \sqrt{\frac{m_t}{m_c}}\frac{V_{td}}{V_{cd}}\chi_{tc}^{u*},
\end{aligned} \tag{A4}$$

where we have dropped $1/t_\beta$ term in the second line. Numerically, we get $\sqrt{m_u/m_c}V_{ud}/|V_{cd}| \approx 0.28$ and $\sqrt{m_t/m_c}|V_{td}/V_{cd}| \approx 0.09$; therefore, χ_{21}^L is dominated by χ_{cc}^{u*}. Nevertheless, with the result of $\sqrt{2}m_c V_{cd}/v \approx -1.6\times10^{-3}$, the C_{cd}^L effect is 2 orders of magnitude smaller than the contribution of the W boson in the SM. This contribution can be ignored for a phenomenological analysis. Similarly, we write C_{cd}^R as

$$\begin{aligned}
\frac{\sqrt{2}}{v}C_{cd}^R = \frac{\sqrt{2}}{v}\Bigg[&t_\beta m_d V_{cd}\left(1 - \frac{\chi_{11}^d}{s_\beta}\right) - \frac{\sqrt{m_s m_d}}{c_\beta}\chi_{21}^d V_{cs}\\
&- \frac{\sqrt{m_b m_d}}{c_\beta}\chi_{31}^d V_{cb}\Bigg].
\end{aligned} \tag{A5}$$

Using $t_\beta \sim 50$, we find that the first, second, and third terms in C^R_{cd} are around 1.3×10^{-3} with $|1-\chi^d_{11}/s_\beta|=2$, 9.1×10^{-3}, and 2.5×10^{-3}, respectively; that is, C^R_{cd} is dominated by the χ^d_{sd} term and can be one order smaller than the SM gauge coupling of $(g/\sqrt{2})V_{cd}$. Taking the case with $1/c_\beta \approx t_\beta$, a simple expression can be given as

$$\frac{\sqrt{2}}{v}C^R_{cd} \approx -\sqrt{2}\frac{m_d t_\beta}{v}V_{cs}\sqrt{\frac{m_s}{m_d}}\chi^d_{sd} \approx 8.3\times10^{-4} t_\beta \chi^d_{sd} V_{cd}. \tag{A6}$$

c. tdH^+ vertex

The C^L_{td} coupling is expressed as

$$\begin{aligned}\frac{\sqrt{2}}{v}C^L_{td} &= \frac{\sqrt{2}}{v}\left[\left(\frac{1}{t_\beta}-\frac{\chi^{u*}_{tt}}{s_\beta}\right)m_t V_{td} - \frac{\sqrt{m_t m_c}}{s_\beta}\chi^{u*}_{ct}V_{cd} - \frac{\sqrt{m_t m_u}}{s_\beta}\chi^{u*}_{ut}V_{ud}\right]\\ &\approx \sqrt{2}\frac{m_t}{v}V_{td}\left(\frac{1}{t_\beta}-\frac{\chi^L_{td}}{s_\beta}\right),\\ \chi^L_{td} &= \chi^{u*}_{tt} + \sqrt{\frac{m_c}{m_t}}\frac{V_{cd}}{V_{td}}\chi^{u*}_{ct}.\end{aligned} \tag{A7}$$

Since the coefficient of χ^{u*}_{ut} term is a factor of 4 smaller than that of χ^{u*}_{ct}, we dropped the χ^{u*}_{ut} term. From Eq. (A7), it can be seen that the C^L_{td} effect in the generic 2HDM is comparable to the SM coupling of $(g/\sqrt{2})V_{td}$, where χ^L_{td} is the main parameter. Because of $m_d V_{td} \ll \sqrt{m_s m_d}V_{ts} \ll \sqrt{m_b m_d}V_{tb}$, the C^R_{td} Yukawa coupling can be simplified as

$$\frac{\sqrt{2}}{v}C^R_{td} \approx -\sqrt{2}\frac{m_b t_\beta}{v}\sqrt{\frac{m_d}{m_b}}\chi^d_{bd}V_{tb}. \tag{A8}$$

Intriguingly, unlike the case in C^L_{td}, C^R_{td} has no V_{td} suppression; thus, its value with a large t_β scheme can be even larger than $(g/\sqrt{2})V_{td}$ in the SM. Moreover, when χ^{u*}_{tt} and χ^{u*}_{ct} are in the range of $O(0.1)$–$O(1)$, χ^L_{td} in C^L_{td} can be small if the cancellation occurs between χ^{u*}_{tt} and χ^{u*}_{ct}. However, since the cancellation cannot occur in Eq. (A8), χ^d_{bd} will be directly bounded by the rare decays.

d. $u(c)sH^+$ vertex

To analyze the $u(c)$-s-H^+ couplings, $C^{L,R}_{us}$ and $C^{L,R}_{cs}$ can be reduced to be, respectively,

$$\begin{aligned}\frac{\sqrt{2}}{v}C^L_{us} &= \frac{\sqrt{2}}{v}\left[\left(\frac{1}{t_\beta}-\frac{\chi^{u*}_{uu}}{s_\beta}\right)m_u V_{us} - \frac{\sqrt{m_u m_c}}{s_\beta}\chi^{u*}_{cu}V_{cs} - \frac{\sqrt{m_u m_t}}{s_\beta}\chi^{u*}_{tu}V_{ts}\right] \sim O(10^{-4}),\end{aligned} \tag{A9}$$

$$\begin{aligned}\frac{\sqrt{2}}{v}C^L_{cs} &= \frac{\sqrt{2}}{v}\left[\left(\frac{1}{t_\beta}-\frac{\chi^{u*}_{cc}}{s_\beta}\right)m_c V_{cs} - \frac{\sqrt{m_c m_u}}{s_\beta}\chi^{u*}_{uc}V_{us} - \frac{\sqrt{m_c m_t}}{s_\beta}\chi^{u*}_{tc}V_{ts}\right]\\ &\approx -\sqrt{2}\frac{m_c}{v s_\beta}V_{cs}\left(\chi^{u*}_{cc} + \sqrt{\frac{m_t}{m_c}}\frac{V_{ts}}{V_{cs}}\chi^{u*}_{tc}\right)\\ &\approx -\sqrt{2}\frac{m_c}{v s_\beta}V_{cs}(\chi^{u*}_{cc} - 0.45\chi^{u*}_{tc}),\end{aligned} \tag{A10}$$

where $\sqrt{2}C^L_{us}/v$ is around 10^{-4} and is thus negligible. Although $\sqrt{2}m_c/vV_{cs} \sim 7.4\times10^{-4}$, it is still 2 orders smaller than the gauge coupling in the SM. In the phenomenological analysis, the C^L_{cs} effect can be neglected. Similarly, the C^R_{us} and C^R_{cs} couplings can be simplified as

$$\begin{aligned}\frac{\sqrt{2}}{v}C^R_{us} &\approx \sqrt{2}\frac{m_s t_\beta}{v}V_{us}\left(1-\frac{\chi^R_{us}}{s_\beta}\right),\\ \chi^R_{us} &= \chi^d_{ss} + \sqrt{\frac{m_d}{m_s}}\frac{V_{ud}}{V_{us}}\chi^d_{ds},\end{aligned} \tag{A11}$$

$$\begin{aligned}\frac{\sqrt{2}}{v}C^R_{cs} &\approx \sqrt{2}\frac{m_s t_\beta}{v}V_{cs}\left(1-\frac{\chi^R_{cs}}{s_\beta}\right),\\ \chi^R_{cs} &= \chi^d_{ss} + \sqrt{\frac{m_b}{m_s}}\frac{V_{cb}}{V_{cs}}\chi^d_{bs}.\end{aligned} \tag{A12}$$

e. tsH^+ vertex

Using $m_t V_{ts} \sim 6.72$ GeV $< \sqrt{m_c m_t}V_{cs} \sim 14.8$ GeV and $m_s V_{ts} \ll \sqrt{m_s m_b}V_{tb} \sim 0.66$ GeV, we can simplify $C^{L,R}_{ts}$ to be

$$\begin{aligned}\frac{\sqrt{2}}{v}C^L_{ts} &\approx \sqrt{2}\frac{m_t}{v}V_{ts}\left(\frac{1}{t_\beta}-\frac{\chi^L_{ts}}{s_\beta}\right),\\ \chi^L_{ts} &= \chi^{u*}_{tt} + \sqrt{\frac{m_c}{m_t}}\frac{V_{cs}}{V_{ts}}\chi^{u*}_{ct},\\ \frac{\sqrt{2}}{v}C^R_{ts} &\approx -\sqrt{2}\frac{\sqrt{m_b m_s}}{v c_\beta}\chi^d_{bs}V_{tb}.\end{aligned} \tag{A13}$$

It can be seen that, due to the new factor χ^L_{ts}, $\sqrt{2}C^L_{ts}/v$ can be comparable with the SM coupling of $gV_{ts}/\sqrt{2}$ without relying on the large t_β scheme.

2. $\bar{B} \to (D,D^*)$ form factors in the HQET

We summarize the relevant $\bar{B} \to D^{(*)}$ form factors with the corrections of $\Lambda_{QCD}/m_{b,c}$ and α_s, which are shown in Ref. [18]. To describe the $\bar{B} \to (D, D^*)$ transition form factors based on the HQET, it is convenient to use the dimensionless kinetic variables, defined as

$$v = \frac{p_B}{m_B}, \qquad v' = \frac{p_{D^{(*)}}}{m_{D^{(*)}}}, \qquad w = v \cdot v' = \frac{m_B^2 + m_{D^{(*)}}^2 - q^2}{2 m_B m_{D^{(*)}}}. \tag{A14}$$

Thus, the $\bar{B} \to D$ form factors can be defined as

$$\begin{aligned} \langle D|\bar{c}b|\bar{B}\rangle &= \sqrt{m_B m_D} h_S (w+1), \\ \langle D|\bar{c}\gamma^\mu b|\bar{B}\rangle &= \sqrt{m_B m_D}(h_+ (v+v')^\mu + h_- (v-v')^\mu), \\ \langle D|\bar{c}\sigma^{\mu\nu} b|\bar{B}\rangle &= i\sqrt{m_B m_D} h_T (v'^\mu v^\nu - v'^\nu v^\mu), \end{aligned} \tag{A15}$$

while the form factors for $\bar{B} \to D^*$ are

$$\begin{aligned} \langle D^*|\bar{c}\gamma^5 b|\bar{B}\rangle &= -\sqrt{m_B m_{D^*}} h_P \epsilon^* \cdot v, \\ \langle D^*|\bar{c}\gamma^\mu b|\bar{B}\rangle &= i\sqrt{m_B m_{D^*}} h_V \epsilon^{\mu\nu\alpha\beta} \epsilon^*_\nu v'_\alpha v_\beta, \\ \langle D^*|\bar{c}\gamma^\mu\gamma^5 b|\bar{B}\rangle &= \sqrt{m_B m_{D^*}}[h_{A_1}(w+1)\epsilon^{*\mu} \\ &\quad - h_{A_2}(\epsilon^* \cdot v) v^\mu - h_{A_3}(\epsilon^* \cdot v) v'^\mu], \\ \langle D^*|\bar{c}\sigma^{\mu\nu} b|\bar{B}\rangle &= -\sqrt{m_B m_{D^*}}[h_{T_1}\epsilon^*_\alpha (v+v')_\beta \\ &\quad + h_{T_2}\epsilon^*_\alpha (v-v')_\beta + h_{T_3}(\epsilon^* \cdot v) v_\alpha v'_\beta], \end{aligned} \tag{A16}$$

where h_-, h_{A_2}, and $h_{T_{2,3}}$ vanish in the heavy quark limit and the remaining form factors are equal to the leading-order Isgur-Wise function $\xi(w)$.

We take the parametrization of the leading-order Isgur-Wise function as [18,124]

$$\frac{\xi(w)}{\xi(w_0)} \simeq 1 - 8a^2\bar{\rho}_*^2 z_* + [V_{21}\bar{\rho}_*^2 - V_{20} + \Delta(e_b, e_c, \alpha_s)] z_*^2, \tag{A17}$$

where $V_{21} = 57.0$, $V_{20} = 7.5$; z_* and a are defined, respectively, as [124]

$$z_* = \frac{\sqrt{w+1} - \sqrt{2}a}{\sqrt{w+1} + \sqrt{2}a}, \qquad a = \sqrt{\frac{1+r_D}{2\sqrt{r_D}}}, \tag{A18}$$

$r_D = m_D/m_B$, w_0 is determined from $z(w_0) = 0$; $\bar{\rho}_*^2$ is the slope parameter of $\xi(w)/\xi(w_0)$, and $\Delta(e_b, e_c, \alpha_s)$ denotes the correction effects of $O(e_{b,c})$ with $e_{b(c)} = \bar{\Lambda}/m_{b(c)}$ and $O(\alpha_s)$. We take the results using the fit scenario of th: $L_{w\geq 1}$ + SR shown in Ref. [18]. In addition to $\bar{\rho}_*^2 = 1.24 \pm 0.08$, the values of subleading Isgur-Wise functions at $w = 1$ are given in Table IV. Using these results, the correction of $O(e_{b,c})$ and $O(\alpha_s)$ can be obtained as

$$\Delta(e_b, e_c, \alpha_s) \approx 0.582 \pm 0.298, \tag{A19}$$

where we adopt the $1S$ scheme for m_b and use the value of $m_b^{1S} = 4.71 \pm 0.05$ GeV [18]. In addition, $\delta m_{bc} = m_b - m_c = 3.40 \pm 0.02$ GeV and $\bar{\Lambda} = 0.45$ GeV are used.

Following the notation in Ref. [18], the form factors up to $O(e_{b,c})$ and $O(\alpha_s)$ can be expressed by factoring out ξ as $h_i = \hat{h}_i \xi$, where the $\hat{h}_i$ for the $\bar{B} \to D$ decay are given as [18]

$$\hat{h}_+ = 1 + \hat{\alpha}_s\left[C_{V_1} + \frac{w+1}{2}(C_{V_1} + C_{V_3})\right] + (e_c + e_b)\hat{L}_1, \tag{A20a}$$

$$\hat{h}_- = \hat{\alpha}_s \frac{w+1}{2}(C_{V_2} - C_{V_3}) + (e_c - e_b)\hat{L}_4, \tag{A20b}$$

$$\hat{h}_S = 1 + \hat{\alpha}_s C_S + (e_c + e_b)\left[\hat{L}_1 - \hat{L}_4 \frac{w-1}{w+1}\right], \tag{A20c}$$

$$\hat{h}_T = 1 + \hat{\alpha}_s(C_{T_1} - C_{T_2} + C_{T_3}) + (e_c + e_b)(\hat{L}_1 - \hat{L}_4); \tag{A20d}$$

for $\bar{B} \to D^*$, the associated $\hat{h}_i$ are shown as [18]

$$\hat{h}_V = 1 + \alpha_s C_{V_1} + e_c(\hat{L}_2 - \hat{L}_5) + e_b(\hat{L}_1 - \hat{L}_4), \tag{A21a}$$

$$\hat{h}_{A_1} = 1 + \hat{\alpha}_s C_{A_1} + e_c\left(\hat{L}_2 - \hat{L}_5 \frac{w-1}{w+1}\right) + e_b\left(\hat{L}_1 - \hat{L}_4 \frac{w-1}{w+1}\right), \tag{A21b}$$

$$\hat{h}_{A_2} = \hat{\alpha}_s C_{A_2} + e_c(\hat{L}_3 + \hat{L}_6), \tag{A21c}$$

TABLE IV. The results of subleading Isgur-Wise functions using the fit scenario of th: $L_{w\geq 1}$ + SR.

FS	$\hat{\chi}_2(1)$	$\hat{\chi}'_2(1)$	$\hat{\chi}'_3(1)$	$\eta(1)$	$\eta'(1)$
th: $L_{w\geq 1}$ + SR	-0.06 ± 0.02	-0.00 ± 0.02	0.04 ± 0.02	0.31 ± 0.04	0.05 ± 0.10

$$\hat{h}_{A_3} = 1 + \hat{\alpha}_s(C_{A_1} + C_{A_3}) + e_c(\hat{L}_2 - \hat{L}_3 + \hat{L}_6 - \hat{L}_5) + e_b(\hat{L}_1 - \hat{L}_4), \tag{A21d}$$

$$\hat{h}_P = 1 + \hat{\alpha}_s C_P + e_c[\hat{L}_2 + \hat{L}_3(w-1) + \hat{L}_5 - \hat{L}_6(w+1)] + e_b(\hat{L}_1 - \hat{L}_4), \tag{A21e}$$

$$\hat{h}_{T_1} = 1 + \hat{\alpha}_s\left[C_{T_1} + \frac{w-1}{2}(C_{T_2} - C_{T_3})\right] + e_c\hat{L}_2 + e_b\hat{L}_1, \tag{A21f}$$

$$\hat{h}_{T_2} = \hat{\alpha}_s\frac{w+1}{2}(C_{T_2} + C_{T_3}) + e_c\hat{L}_5 - e_b\hat{L}_4, \tag{A21g}$$

$$\hat{h}_{T_3} = \hat{\alpha}_s C_{T_2} + e_c(\hat{L}_6 - \hat{L}_3). \tag{A21h}$$

The w-dependent functions C_{Γ_i} can be found in Refs. [18,125], and the subleading Isgur-Wise functions are [122]

$$\hat{L}_1 = -4(w-1)\hat{\chi}_2 + 12\hat{\chi}_3, \quad \hat{L}_2 = -4\hat{\chi}_3, \quad \hat{L}_3 = 4\hat{\chi}_2, \quad \hat{L}_4 = 2\eta - 1, \quad \hat{L}_5 = -1, \quad \hat{L}_6 = -2\frac{1+\eta}{w+1}, \tag{A22}$$

where the w-dependent functions $\hat{\chi}_i$ and η can be approximated, respectively, as

$$\hat{\chi}_2(w) \simeq \hat{\chi}_2(1) + \hat{\chi}_2'(1)(w-1), \quad \hat{\chi}_3(w) \simeq \hat{\chi}_3'(1)(w-1), \quad \eta(w) \simeq \eta(1) + \eta'(1)(w-1). \tag{A23}$$

[1] T. D. Lee, Phys. Rev. D **8**, 1226 (1973).
[2] R. D. Peccei and H. R. Quinn, Phys. Rev. Lett. **38**, 1440 (1977).
[3] J. F. Gunion, H. E. Haber, G. L. Kane, and S. Dawson, Front. Phys. **80**, 1 (2000).
[4] C. H. Chen and T. Nomura, Phys. Rev. D **90**, 075008 (2014).
[5] R. Benbrik, C. H. Chen, and T. Nomura, Phys. Rev. D **93**, 095004 (2016).
[6] C. H. Chen and T. Nomura, Phys. Lett. B **767**, 443 (2017).
[7] G. C. Branco, P. M. Ferreira, L. Lavoura, M. N. Rebelo, M. Sher, and J. P. Silva, Phys. Rep. **516**, 1 (2012).
[8] J. P. Lees *et al.* (*BABAR* Collaboration), Phys. Rev. Lett. **109**, 101802 (2012).
[9] J. P. Lees *et al.* (*BABAR* Collaboration), Phys. Rev. D **88**, 072012 (2013).
[10] M. Huschle *et al.* (Belle Collaboration), Phys. Rev. D **92**, 072014 (2015).
[11] A. Abdesselam *et al.* (Belle Collaboration), arXiv:1603.06711.
[12] S. Hirose *et al.* (Belle Collaboration), Phys. Rev. Lett. **118**, 211801 (2017).
[13] R. Aaij *et al.* (LHCb Collaboration), Phys. Rev. Lett. **115**, 111803 (2015); **115**, 159901(E) (2015).
[14] R. Aaij *et al.* (LHCb Collaboration), Phys. Rev. Lett. **120**, 171802 (2018).
[15] Y. Amhis *et al.* (HFLAV Collaboration), Eur. Phys. J. C **77**, 895 (2017).
[16] J. A. Bailey *et al.* (MILC Collaboration), Phys. Rev. D **92**, 034506 (2015).
[17] H. Na, C. M. Bouchard, G. P. Lepage, C. Monahan, and J. Shigemitsu (HPQCD Collaboration), Phys. Rev. D **92**, 054510 (2015); **93**, 119906 (2016).
[18] F. U. Bernlochner, Z. Ligeti, M. Papucci, and D. J. Robinson, Phys. Rev. D **95**, 115008 (2017).
[19] S. Jaiswal, S. Nandi, and S. K. Patra, J. High Energy Phys. 12 (2017) 060.
[20] S. Fajfer, J. F. Kamenik, and I. Nisandzic, Phys. Rev. D **85**, 094025 (2012).
[21] D. Bigi, P. Gambino, and S. Schacht, J. High Energy Phys. 11 (2017) 061.
[22] S. Fajfer, J. F. Kamenik, I. Nisandzic, and J. Zupan, Phys. Rev. Lett. **109**, 161801 (2012).
[23] A. Crivellin, C. Greub, and A. Kokulu, Phys. Rev. D **86**, 054014 (2012).
[24] A. Datta, M. Duraisamy, and D. Ghosh, Phys. Rev. D **86**, 034027 (2012).
[25] J. A. Bailey *et al.*, Phys. Rev. Lett. **109**, 071802 (2012).
[26] A. Celis, M. Jung, X. Q. Li, and A. Pich, J. High Energy Phys. 01 (2013) 054.
[27] M. Tanaka and R. Watanabe, Phys. Rev. D **87**, 034028 (2013).
[28] J. Hernandez-Sanchez, S. Moretti, R. Noriega-Papaqui, and A. Rosado, J. High Energy Phys. 07 (2013) 044.
[29] P. Biancofiore, P. Colangelo, and F. De Fazio, Phys. Rev. D **87**, 074010 (2013).
[30] A. Crivellin, A. Kokulu, and C. Greub, Phys. Rev. D **87**, 094031 (2013).
[31] I. Dorsner, S. Fajfer, N. Kosnik, and I. Nisandzic, J. High Energy Phys. 11 (2013) 084.
[32] R. Dutta, A. Bhol, and A. K. Giri, Phys. Rev. D **88**, 114023 (2013).
[33] Y. Sakaki, M. Tanaka, A. Tayduganov, and R. Watanabe, Phys. Rev. D **88**, 094012 (2013).
[34] B. Bhattacharya, A. Datta, D. London, and S. Shivashankara, Phys. Lett. B **742**, 370 (2015).
[35] R. Alonso, B. Grinstein, and J. Martin Camalich, J. High Energy Phys. 10 (2015) 184.
[36] L. Calibbi, A. Crivellin, and T. Ota, Phys. Rev. Lett. **115**, 181801 (2015).

[37] M. Freytsis, Z. Ligeti, and J. T. Ruderman, Phys. Rev. D **92**, 054018 (2015).
[38] A. Crivellin, J. Heeck, and P. Stoffer, Phys. Rev. Lett. **116**, 081801 (2016).
[39] S. Bhattacharya, S. Nandi, and S. K. Patra, Phys. Rev. D **93**, 034011 (2016).
[40] R. Alonso, A. Kobach, and J. Martin Camalich, Phys. Rev. D **94**, 094021 (2016).
[41] D. Das, C. Hati, G. Kumar, and N. Mahajan, Phys. Rev. D **94**, 055034 (2016).
[42] X. Q. Li, Y. D. Yang, and X. Zhang, J. High Energy Phys. 08 (2016) 054.
[43] S. M. Boucenna, A. Celis, J. Fuentes-Martin, A. Vicente, and J. Virto, J. High Energy Phys. 12 (2016) 059.
[44] D. Becirevic, S. Fajfer, N. Kosnik, and O. Sumensari, Phys. Rev. D **94**, 115021 (2016).
[45] W. Altmannshofer, S. Gori, S. Profumo, and F. S. Queiroz, J. High Energy Phys. 12 (2016) 106.
[46] B. Bhattacharya, A. Datta, J. P. Guevin, D. London, and R. Watanabe, J. High Energy Phys. 01 (2017) 015.
[47] D. Bardhan, P. Byakti, and D. Ghosh, J. High Energy Phys. 01 (2017) 125.
[48] R. Dutta and A. Bhol, Phys. Rev. D **96**, 036012 (2017).
[49] S. Bhattacharya, S. Nandi, and S. K. Patra, Phys. Rev. D **95**, 075012 (2017).
[50] R. Alonso, B. Grinstein, and J. Martin Camalich, Phys. Rev. Lett. **118**, 081802 (2017).
[51] R. Dutta and A. Bhol, Phys. Rev. D **96**, 076001 (2017).
[52] C. H. Chen, T. Nomura, and H. Okada, Phys. Lett. B **774**, 456 (2017).
[53] C. H. Chen and T. Nomura, Eur. Phys. J. C **77**, 631 (2017).
[54] E. Megias, M. Quiros, and L. Salas, J. High Energy Phys. 07 (2017) 102.
[55] A. Crivellin, D. Muller, and T. Ota, J. High Energy Phys. 09 (2017) 040.
[56] W. Altmannshofer, P. Stangl, and D. M. Straub, Phys. Rev. D **96**, 055008 (2017).
[57] M. Ciuchini, A. M. Coutinho, M. Fedele, E. Franco, A. Paul, L. Silvestrini, and M. Valli, Eur. Phys. J. C **77**, 688 (2017).
[58] A. Celis, J. Fuentes-Martin, A. Vicente, and J. Virto, Phys. Rev. D **96**, 035026 (2017).
[59] J. F. Kamenik, Y. Soreq, and J. Zupan, Phys. Rev. D **97**, 035002 (2018).
[60] W. Altmannshofer, P. S. B. Dev, and A. Soni, Phys. Rev. D **96**, 095010 (2017).
[61] A. K. Alok, D. Kumar, J. Kumar, and R. Sharma, arXiv: 1704.07347.
[62] D. Choudhury, A. Kundu, R. Mandal, and R. Sinha, Phys. Rev. Lett. **119**, 151801 (2017).
[63] D. Buttazzo, A. Greljo, G. Isidori, and D. Marzocca, J. High Energy Phys. 11 (2017) 044.
[64] C. H. Chen and T. Nomura, Phys. Lett. B **777**, 420 (2018).
[65] A. G. Akeroyd and C. H. Chen, Phys. Rev. D **96**, 075011 (2017).
[66] S. Iguro and K. Tobe, Nucl. Phys. **B925**, 560 (2017).
[67] J. A. Bailey *et al.* (Fermilab Lattice and MILC Collaborations), Phys. Rev. D **92**, 014024 (2015).
[68] P. Ball and R. Zwicky, Phys. Rev. D **71**, 014015 (2005).
[69] P. Ball, Phys. Lett. B **644**, 38 (2007).
[70] C. Patrignani *et al.* (Particle Data Group), Chin. Phys. C **40**, 100001 (2016).
[71] G. Isidori and P. Paradisi, Phys. Lett. B **639**, 499 (2006).
[72] C. H. Chen and C. Q. Geng, J. High Energy Phys. 10 (2006) 053.
[73] A. G. Akeroyd and C. H. Chen, Phys. Rev. D **75**, 075004 (2007).
[74] A. G. Akeroyd, C. H. Chen, and S. Recksiegel, Phys. Rev. D **77**, 115018 (2008).
[75] M. Misiak and M. Steinhauser, Eur. Phys. J. C **77**, 201 (2017).
[76] Y. H. Ahn and C. H. Chen, Phys. Lett. B **690**, 57 (2010).
[77] T. P. Cheng and M. Sher, Phys. Rev. D **35**, 3484 (1987).
[78] K. S. Babu and C. F. Kolda, Phys. Rev. Lett. **84**, 228 (2000).
[79] G. Isidori and A. Retico, J. High Energy Phys. 11 (2001) 001.
[80] G. Isidori and A. Retico, J. High Energy Phys. 09 (2002) 063.
[81] A. Dedes, J. R. Ellis, and M. Raidal, Phys. Lett. B **549**, 159 (2002).
[82] A. Sibidanov *et al.* (Belle Collaboration), Phys. Rev. Lett. **121**, 031801 (2018).
[83] T. Abe *et al.* (Belle-II Collaboration), arXiv:1011.0352.
[84] R. Aaij *et al.* (LHCb Collaboration), Phys. Rev. Lett. **113**, 151601 (2014).
[85] R. Aaij *et al.* (LHCb Collaboration), J. High Energy Phys. 08 (2017) 055.
[86] M. Hussain, M. Usman, M. A. Paracha, and M. J. Aslam, Phys. Rev. D **95**, 075009 (2017).
[87] P. Arnan, D. Becirevic, F. Mescia, and O. Sumensari, Eur. Phys. J. C **77**, 796 (2017).
[88] A. Arbey, F. Mahmoudi, O. Stal, and T. Stefaniak, Eur. Phys. J. C **78**, 182 (2018).
[89] A. Arhrib, R. Benbrik, C. H. Chen, J. K. Parry, L. Rahili, S. Semlali, and Q. S. Yan, arXiv:1710.05898.
[90] D. Choudhury, A. Kundu, R. Mandal, and R. Sinha, Nucl. Phys. **B933**, 433 (2018).
[91] S. Iguro and Y. Omura, J. High Energy Phys. 05 (2018) 173.
[92] J. Kalinowski, Phys. Lett. B **245**, 201 (1990).
[93] M. Tanaka and R. Watanabe, Phys. Rev. D **82**, 034027 (2010).
[94] U. Nierste, S. Trine, and S. Westhoff, Phys. Rev. D **78**, 015006 (2008).
[95] R. Alonso, J. Martin Camalich, and S. Westhoff, Phys. Rev. D **95**, 093006 (2017).
[96] D. Becirevic, M. Ciuchini, E. Franco, V. Giménez, G. Martinelli, A. Masiero, M. Papinutto, J. Reyes, and L. Silvestrini, Nucl. Phys. **B634**, 105 (2002).
[97] J. Urban, F. Krauss, U. Jentschura, and G. Soff, Nucl. Phys. **B523**, 40 (1998).
[98] E. Gamiz, C. T. H. Davies, G. P. Lepage, J. Shigemitsu, and M. Wingate (HPQCD Collaboration), Phys. Rev. D **80**, 014503 (2009).
[99] A. Bazavov *et al.*, Phys. Rev. D **86**, 034503 (2012).
[100] Y. Aoki, T. Ishikawa, T. Izubuchi, C. Lehner, and A. Soni, Phys. Rev. D **91**, 114505 (2015).
[101] S. Aoki *et al.*, Eur. Phys. J. C **77**, 112 (2017).

[102] D. Becirevic, V. Gimenez, G. Martinelli, M. Papinutto, and J. Reyes, J. High Energy Phys. 04 (2002) 025.
[103] D. Becirevic, V. Gimenez, G. Martinelli, M. Papinutto, and J. Reyes, Nucl. Phys. B, Proc. Suppl. **106**, 385 (2002).
[104] N. Carrasco *et al.* (ETM Collaboration), J. High Energy Phys. 03 (2014) 016.
[105] G. Buchalla, A. J. Buras, and M. E. Lautenbacher, Rev. Mod. Phys. **68**, 1125 (1996).
[106] A. Lenz, U. Nierste, J. Charles, S. Descotes-Genon, A. Jantsch, C. Kaufhold, H. Lacker, S. Monteil, V. Niess, and S. T'Jampens, Phys. Rev. D **83**, 036004 (2011).
[107] B. Colquhoun, C. T. H. Davies, J. Kettle, J. Koponen, A. T. Lytle, R. J. Dowdall, and G. P. Lepage (HPQCD Collaboration), Phys. Rev. D **91**, 114509 (2015).
[108] A. J. Buras, M. Jamin, and P. H. Weisz, Nucl. Phys. **B347**, 491 (1990).
[109] M. Ciuchini, E. Franco, V. Lubicz, G. Martinelli, I. Scimemi, and L. Silvestrini, Nucl. Phys. **B523**, 501 (1998).
[110] A. J. Buras, M. Misiak, and J. Urban, Nucl. Phys. **B586**, 397 (2000).
[111] M. Czakon, P. Fiedler, T. Huber, M. Misiak, T. Schutzmeier, and M. Steinhauser, J. High Energy Phys. 04 (2015) 168.
[112] M. Misiak *et al.*, Phys. Rev. Lett. **114**, 221801 (2015).
[113] M. Blanke, A. J. Buras, K. Gemmler, and T. Heidsieck, J. High Energy Phys. 03 (2012) 024.
[114] A. J. Buras, L. Merlo, and E. Stamou, J. High Energy Phys. 08 (2011) 124.
[115] M. Ciuchini, G. Degrassi, P. Gambino, and G. F. Giudice, Nucl. Phys. **B527**, 21 (1998).
[116] F. Borzumati and C. Greub, Phys. Rev. D **58**, 074004 (1998).
[117] F. Borzumati and C. Greub, Phys. Rev. D **59**, 057501 (1999).
[118] T. Hermann, M. Misiak, and M. Steinhauser, J. High Energy Phys. 11 (2012) 036.
[119] E. Dalgic, A. Gray, M. Wingate, C. T. H. Davies, G. P. Lepage, and J. Shigemitsu, Phys. Rev. D **73**, 074502 (2006); **75**, 119906(E) (2007).
[120] J. M. Flynn, T. Izubuchi, T. Kawanai, C. Lehner, A. Soni, R. S. Van de Water, and O. Witzel, Phys. Rev. D **91**, 074510 (2015).
[121] P. Ball and R. Zwicky, Phys. Rev. D **71**, 014029 (2005).
[122] A. F. Falk and M. Neubert, Phys. Rev. D **47**, 2965 (1993).
[123] D. A. Faroughy, A. Greljo, and J. F. Kamenik, Phys. Lett. B **764**, 126 (2017).
[124] I. Caprini, L. Lellouch, and M. Neubert, Nucl. Phys. **B530**, 153 (1998).
[125] M. Neubert, Nucl. Phys. **B371**, 149 (1992).